UCLA
UCLA Previously Published Works

Title

Patronin-mediated minus end growth is required for dendritic microtubule polarity

Permalink

https://escholarship.org/uc/item/5h54t0d0

Journal

Journal of Cell Biology, 218(7)

ISSN

0021-9525

Authors

Feng, Chengye
Thyagarajan, Pankajam
Shorey, Matthew
et al.

Publication Date

2019-07-01

DOI

10.1083/jcb.201810155

Peer reviewed

ARTICLE

Patronin-mediated minus end growth is required for dendritic microtubule polarity

Chengye Feng[1], Pankajam Thyagarajan[1] , Matthew Shorey[1], Dylan Y. Seebold[1], Alexis T. Weiner[1] , Richard M. Albertson[1], Kavitha S. Rao[1], Alvaro Sagasti[2], Daniel J. Goetschius[1], and Melissa M. Rolls[1]

Microtubule minus ends are thought to be stable in cells. Surprisingly, in *Drosophila* and zebrafish neurons, we observed persistent minus end growth, with runs lasting over 10 min. In *Drosophila*, extended minus end growth depended on Patronin, and Patronin reduction disrupted dendritic minus-end-out polarity. In fly dendrites, microtubule nucleation sites localize at dendrite branch points. Therefore, we hypothesized minus end growth might be particularly important beyond branch points. Distal dendrites have mixed polarity, and reduction of Patronin lowered the number of minus-end-out microtubules. More strikingly, extra Patronin made terminal dendrites almost completely minus-end-out, indicating low Patronin normally limits minus-end-out microtubules. To determine whether minus end growth populated new dendrites with microtubules, we analyzed dendrite development and regeneration. Minus ends extended into growing dendrites in the presence of Patronin. In sum, our data suggest that Patronin facilitates sustained microtubule minus end growth, which is critical for populating dendrites with minus-end-out microtubules.

Introduction

Microtubule plus ends exhibit rapid growth and shrinkage phases, a behavior termed dynamic instability (Mitchison and Kirschner, 1984). This behavior occurs in vitro with pure αβtubulin dimers and in vivo, where it can be regulated by plus end binding proteins and microtubule age (Gardner et al., 2013; Akhmanova and Steinmetz, 2015; Brouhard, 2015). Minus ends also exhibit dynamic instability in vitro, although their growth rate is two to three times slower than plus ends (Mitchison and Kirschner, 1984; Dammermann et al., 2003). In vivo, however, minus ends are generally thought not to contribute to microtubule dynamics or exploration of cellular space (Akhmanova and Steinmetz, 2015).

In cells, the γtubulin ring complex acts as a template and nucleator to allow new microtubules to form. As long as it remains attached at the nucleating or minus end, it acts as a cap to block addition of subunits and prevent depolymerization. Free minus ends can then be generated by severing proteins (Baas et al., 2005; Sharp and Ross, 2012). Two well-established fates for free minus ends are depolymerization and stabilization (Dammermann et al., 2003; Akhmanova and Hoogenraad, 2015). In plants, cortical microtubules that are freed from nucleation sites depolymerize at the minus end while growing at the plus end to generate treadmilling behavior (Shaw et al., 2003;

Nakamura et al., 2018). In animal cells, depolymerization at the minus end is an important aspect of mitotic spindle dynamics (Wittmann et al., 2001), and minus end recognition by ASPM (abnormal spindle-like microcephaly associated) is important to help control depolymerization (Jiang et al., 2017). In interphase, most free minus ends seem to be rapidly stabilized by calmodulin-regulated spectrin-associated protein (CAMSAP)/Patronin proteins (Akhmanova and Steinmetz, 2015).

Identification of CAMSAP/Patronin proteins was a major breakthrough in understanding the cellular stability of minus ends. They were the first proteins identified that could directly recognize free minus ends (Akhmanova and Hoogenraad, 2015) and are likely responsible for their resistance to depolymerization in interphase (Dammermann et al., 2003; Jiang et al., 2014; Akhmanova and Hoogenraad, 2015). The repertoire of minus end–binding proteins was recently expanded by the addition of ASPM, which can also recognize minus ends and controls their depolymerization in the spindle (Jiang et al., 2017). It is not known whether this family of proteins also functions in postmitotic cells like neurons.

Invertebrates have one CAMSAP/Patronin family member, termed Patronin, while vertebrates generally have three, CAMSAP1–3, with some extras where genome duplications have

occurred (King et al., 2014). For example, in zebrafish, there are two each of CAMSAP1 and 2 and one CAMSAP3 (King et al., 2014). *Drosophila melanogaster* Patronin stabilizes minus ends against depolymerization by kinesin-13 in cultured cells and in vitro (Goodwin and Vale, 2010). Mammalian CAMSAPs also protect minus ends from depolymerization by kinesin-13s in vitro (Hendershott and Vale, 2014) and in cells (Jiang et al., 2014). Overall stabilization of minus ends by CAMSAPs and Patronin is agreed upon as a critical function without which the microtubule network in cultured *Drosophila* cells and mammalian cells including neurons is dramatically destabilized (Goodwin and Vale, 2010; Jiang et al., 2014; Yau et al., 2014).

The relationship between CAMSAPs/Patronin and minus end growth is more complex. In vitro CAMSAP2 and 3, as well as two domains of Patronin, suppress addition of tubulin subunits to the minus end in a concentration-dependent manner (Hendershott and Vale, 2014; Jiang et al., 2014). In contrast, CAMSAP1 tracks minus ends as they grow without altering the rate of subunit addition (Hendershott and Vale, 2014). In cells, CAMSAP1 also tracks growing minus ends, but reduction of CAMSAP1 does not result in any change in microtubule behavior (Jiang et al., 2014). CAMSAP2 has been described as suppressing minus end growth (Hendershott and Vale, 2014) and also as promoting addition of short stretches of microtubule to the minus end (Jiang et al., 2014). Although these two models for CAMSAP2 sound incompatible, they are actually not so different. Minus ends grow slowly in the presence of CAMSAP2 (Hendershott and Vale, 2014; Jiang et al., 2014), and this allows short stretches of CAMSAP2 to become stably associated with the microtubule (Jiang et al., 2014). The stretches are on average 1 μm in control cells and 2 μm when katanin is depleted (Jiang et al., 2014), and so, although they are derived from tubulin subunit addition, this does not result in much net growth at the minus end. In primary neuron cultures, stretches >10 μm of CAMSAP2 along microtubules have been observed, but growth has only been tracked for stretches of about a micron, so it is not clear how the longer stretches arise (Yau et al., 2014). Thus, it is still ambiguous whether extended growth at the minus end occurs in cells and, if so, how it contributes to global microtubule organization.

CAMSAP/Patronin proteins are particularly important in neurons where most, if not all, microtubules are non-centrosomal. In cultured hippocampal neurons, reduction of CAMSAP2, the major family member in this cell type, destabilizes microtubules and reduces dendrite complexity (Yau et al., 2014). *Caenorhabditis elegans* Patronin is required for maintenance of normal neuronal morphology (Marcette et al., 2014), neuronal microtubule stability (Chuang et al., 2014; Richardson et al., 2014), and axon regeneration (Chuang et al., 2014). Beyond stabilizing microtubules, it is not clear whether Patronin regulates specific aspects of microtubule organization in neurons. In epithelial cells, CAMSAP3 is responsible not only for stability of microtubules but also their polarized arrangement with minus ends concentrated at the apical surface (Meng et al., 2008; Noordstra et al., 2016; Toya et al., 2016). Neuronal microtubules are even more dramatically polarized than epithelial ones, with uniform plus-end-out polarity in axons and

mixed or minus-end-out polarity in dendrites (Baas and Lin, 2011). We therefore hypothesized that CAMSAP/Patronin proteins might function to control not only microtubule stability in neurons, but also their polarity.

Drosophila dendrites are strikingly polarized with >90% minus-end-out microtubules (Rolls et al., 2007; Stone et al., 2008). It is conceptually straightforward to imagine plus-end-out processes in which fast-growing microtubule plus ends allow microtubules to populate an extending structure, while more complex models are thought to be required for population of processes with minus-end-out microtubules. In dendrites, local nucleation can generate new minus ends (Ori-McKenney et al., 2012; Nguyen et al., 2014; Yau et al., 2014), and outgrowth of minus ends has not been considered as an alternative way to get minus-end-out microtubules into dendrites. However, in *Drosophila* neurons, nucleation sites are concentrated at dendrite branch points (Ori-McKenney et al., 2012; Nguyen et al., 2014), so how the terminal dendrite beyond the branch point is populated with minus-end-out microtubules remains a conundrum.

Using live imaging of microtubule dynamics with tagged end-binding (EB) proteins in *Drosophila* and zebrafish neurons, we identified a population of slow-growing microtubule ends that move in the opposite direction to fast-growing plus ends. In *Drosophila* dendrites, these slow-moving structures are labeled with Patronin, confirming that they are growing microtubule minus ends. We demonstrate that sustained growth of minus ends requires Patronin, and in turn is important for getting minus-end-out microtubules into distal regions of mature dendrites, as well as into developing and regenerating dendrites.

Results

EB proteins track two types of puncta in sensory neurons of *Drosophila* and zebrafish

EB proteins have been used to track microtubule plus end growth in mammalian neurons in culture and in vivo (Stepanova et al., 2003; Kleele et al., 2014), and neurons in vivo in zebrafish (Lee et al., 2017), *C. elegans* (Goodwin et al., 2012), and *Drosophila* (Stone et al., 2008). In all axons, EB comets move away from the cell body (Baas and Lin, 2011). Dendrites in mammals contain comets that move in both directions (Stepanova et al., 2003; Yau et al., 2016), while in *C. elegans* and *Drosophila*, they move primarily toward the cell body (Stone et al., 2008; Goodwin et al., 2012). The polarity measured with plus end dynamics matches overall polarity of microtubules with one exception: in mammalian neurons, minus-end-out microtubules are slightly underrepresented by dynamic plus ends in dendrites, consistent with minus-end-out microtubules having a longer, more stable region behind the dynamic plus end (Yau et al., 2016; Tas et al., 2017). In *Drosophila* dendrites, monitoring dynamic plus ends predicts the layout of all microtubules, including stable regions (Stone et al., 2008).

Drosophila ddaE neurons are particularly amenable to imaging neuronal microtubule dynamics in vivo as their cell body, dendrite arbor, and proximal axon are all located near the surface of the animal (Fig. 1 A). These cells are proprioceptive dendritic arborization neurons (Hughes and Thomas, 2007) and

Feng et al.
Microtubule minus ends grow into dendrites

Journal of Cell Biology 2310
https://doi.org/10.1083/jcb.201810155

have a relatively simple stereotyped dendrite arbor (Grueber et al., 2003b; Fig. 1 D). While imaging growing microtubules with EB1-GFP, we noticed an unexpected class of moving dots. In addition to the fast-moving comets characteristic of microtubule plus ends, we observed dimmer round dots that moved slowly and processively (Fig. 1 E and Video 1). When plotted by speed, the EB1 dots fell into two clear groups (Fig. 1 B). We therefore used speed to categorize the dots, and the cutoff between the two groups was 1.6 μm per minute. The fast and slow dots moved in largely opposite directions, with most slow dots moving away from the cell body and fast ones moving toward it (Fig. 1, C and E–G). We hypothesized that the slow dots could be growing microtubule minus ends based on their similarity to growing minus ends in vitro (Bieling et al., 2007). Consistent with the idea that EB1-GFP was tracking growing plus and minus ends, we occasionally observed a plus end comet initiating from a slow-moving dot (Fig. 1 G and and Video 2). Similar behavior of fast- and slow-moving EB1-GFP puncta was observed in axons, with the exception that the fast-moving dots moved away from the cell body and slow-moving ones toward it (Fig. 1, H and I).

As the possibility that neurons might contain growing minus ends was unexpected, we wished to determine whether the phenomenon was specific to *Drosophila* or more generally found in neurons. We chose zebrafish for comparison, as they are also amenable to live imaging. Rohon-Beard (RB) neurons are the sensory neurons in larval zebrafish and have previously been used for imaging microtubule growth (Lee et al., 2017). The RB sensory endings are branched and similar to *Drosophila* dendritic arborization neurons (Fig. 1, J–L) with the exception that their microtubules are organized with plus-end-out polarity (Lee et al., 2017). We expressed EB3-GFP in RB neurons and again saw two types of labeled dots (Fig. 1 M and Video 3). The fast-moving ones did not move quite as quickly as in *Drosophila* (Fig. 1 N), but were still clearly distinct from a slow-moving pool similar to that seen in *Drosophila*. For zebrafish, the cutoff used to separate fast and slow dots was 1.3 μm per minute. As expected for plus ends, the fast puncta moved mostly away from the cell body (Fig. 1 O). In contrast, the slow dots moved toward the cell body (Fig. 1 O). Together, these data from *Drosophila* and zebrafish indicate that EB proteins label two classes of moving structures in neurons. The fast-moving puncta are the microtubule plus ends previously characterized in neurons (Stepanova et al., 2003; Stone et al., 2008; Lee et al., 2017). Both the speed and direction of movement of the slow-moving dots suggested that they could be growing minus ends.

Patronin and EB1 colocalize on growing minus ends and track them independently

Patronin/CAMSAP family proteins recognize microtubule minus ends (Akhmanova and Hoogenraad, 2015). To determine whether slow-moving dots were minus ends, we coexpressed EB1-TagRFP-T with 3xYFP-Patronin (simplified to YFP-Patronin throughout). EB1-TagRFP-T behaves similarly to EB1-GFP and labels fast- and slow-moving spots. The only difference is that with this fluorophore, the two types of dots have similar fluorescence intensity (FI; Fig. 2 D). When YFP-Patronin was expressed at high levels, it labeled the whole microtubule lattice

(Fig. 2 A). We therefore selected a transgenic insertion line in which YFP-Patronin was expressed at low levels (Fig. 2 B). Large immobile puncta that appear and disappear but do not move were still present in some neurons (e.g., arrow in Fig. 2 K), perhaps representing residual lattice labeling or recruitment to some other structure. However, when we focused on moving structures, we were able to detect persistent movement of Patronin dots primarily away from the cell body (Fig. 2, C and D). These mobile Patronin puncta coincided with slow-moving EB1 dots labeled with EB1-TagRFP-T (Fig. 2, C and D), but did not overlap the fast EB1 puncta (Fig. 2, C and D; and Video 4). The localization of Patronin to slow EB1 puncta supports the hypothesis that these are growing minus ends.

To confirm that YFP-Patronin recognizes newly generated minus ends, we used a laser to sever dendrites. The predicted location of new minus ends generated by dendrite severing is indicated with a green arrow in Fig. 2 E. A new spot of YFP-Patronin appeared next to the cut site closer to the cell body as predicted (Fig. 2 F).

We next confirmed that the behavior of YFP-Patronin was similar to that of endogenous Patronin and not a function of overexpression or tag location by using two additional tagged lines. Patronin-Venus has the Venus coding sequence replacing the stop codon of the *Patronin* gene, so that the genomic Patronin locus encodes a tagged protein (Nashchekin et al., 2016). Patronin-Venus fluorescence could be observed in neuronal cell bodies (Fig. S1, A and B) and coincided with slow-moving dots of EB1-TagRFP-T in the cell body (Fig. S1 A). However, it was too dim to visualize in dendrites. EGFP-Patronin was generated from a large genomic region such that the EGFP coding sequence is inserted at the 5′ end of the *Patronin* gene and used to generate flies that contain an extra copy of EGFP-Patronin under control of its own regulatory regions (Takeda et al., 2018). This Patronin transgene labeled slow-moving spots in dendrites that were labeled with EB1-TagRFP-T (Fig. 2 G and Fig. S2 D). Thus, similar moving spots were labeled with all three transgenes.

To determine whether either Patronin or EB1 was required to recruit the other protein to growing minus ends, we knocked each down and tracked the other. Because regulation of microtubule growth and dynamics is important in all cells and during mitosis, we used cell type–specific RNAi (Dietzl et al., 2007) to reduce expression of Patronin and EB1 post-mitotically in a subset of neurons. Like fluorescently tagged proteins, hairpin RNAs were expressed with the Gal4-UAS system so that the labeled cells were the ones subject to RNAi knockdown. Expression of a long hairpin RNA (VDRC24551) targeting EB1 completely eliminated EB1-TagRFP-T signal in ddaE neurons (Fig. 2, H and J), but did not eliminate Patronin-YFP accumulating on slow-growing puncta (Fig. 2 K). To confirm that EB1 RNAi also reduced endogenous EB1, we stained larval skins with anti-EB1 antibody (Rogers et al., 2002). EB1 expression was seen in the ddaE neuron and in glia surrounding the cell body (Fig. S1 D). When EB1 RNAi was expressed in the ddaE neuron, the glial staining surrounded a dark region occupied by the cell body (Fig. S1 D), indicating that endogenous EB1 was also very effectively reduced by the RNAi. Two other proteins that contain the
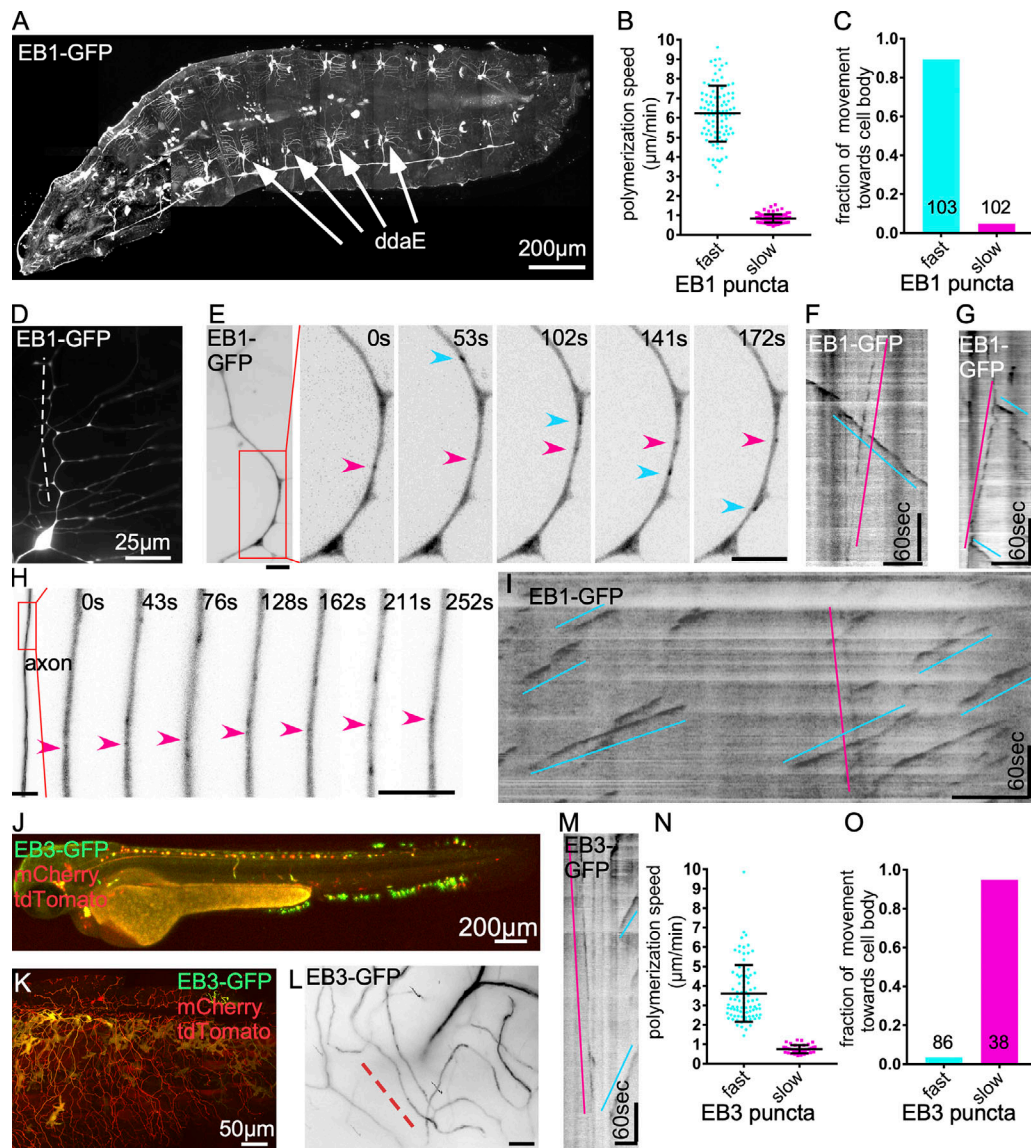
Figure 1.   **EB proteins label two types of puncta in *Drosophila* and zebrafish. (A)** Whole animal image of a 3-d-old larva labeled with EB1-GFP under 221-Gal4. Arrows point to class I ddaE neurons. **(B and C)** Quantification of direction and speed of two types of puncta labeled by EB1-GFP in *Drosophila* ddaE comb dendrites. The speed cutoff between fast and slow puncta was 1.6 µm/min. Numbers on the graphs are total numbers of dots recorded from 16 neurons for fast dots and 35 for slow dots. One neuron was used per animal throughout this study. Error bars are SD for all the graphs presented. Turquoise is used to show fast dots and pink to indicate slow ones in all figures. **(D)** Representative image of a class I ddaE neuron expressing EB1-GFP from a 3-d-old larva. Cell body and dendrites were shown with axon extending to lower left corner toward ventral nerve cord. Dashed line indicates the comb dendrite where observations of EB1-GFP puncta were performed. **(E and F)** Representative image and kymograph of a dendrite segment of a class I ddaE neuron expressing EB1-GFP from a time-lapse recording. Sequential images of the rectangular region are zoomed in to show a slow puncta (pink arrowhead) and a fast one (turquoise arrowhead). Horizontal bars, 5 µm. Vertical bars, 60 s. In all kymographs presented in this study, time flows from top to bottom, and the cell body is on the right side. **(G)** Representative kymograph of two fast dots initiating from a slow-moving one. Horizontal bar, 5 µm. Vertical bar, 60 s. **(H)** Representative image of an axon segment of class IV ddaC neuron expressing EB1-GFP from a time-lapse recording. Sequential images of the rectangular region are zoomed in to focus on a slow dot marked by a pink arrowhead. Multiple fast dots that moved across the same region were not marked. Horizontal bars, 5 µm. **(I)** Kymograph of EB1-GFP in the axon of the ddaC neuron. As in other images, the horizontal bar is 5 µm and vertical is 60 s. Turquoise lines show fast puncta, and pink, slow. The cell body is off the right side of the image. **(J)** Whole animal image of a 48-hpf zebrafish expressing EB3-GFP, tdTomato, and mCherry in RB neurons. EB3-GFP, mCherry, and tdTomato were controlled by the P2X3 and ISL1 promoters. **(K)** Zoomed-in view of RB neurons innervating the skin from the same animal imaged in H. **(L and M)** Representative image and kymograph of sensory endings of an RB neuron expressing EB3-GFP. The dashed line marks the region from which the kymograph was generated. **(N and O)** Quantification of direction and speed of puncta labeled by EB3-GFP in RB neurons of zebrafish. The speed cutoff between fast and slow puncta was 1.2 µm/min. Numbers on the graph are numbers of dots recorded from 6 neurons for fast puncta and 12 for slow puncta.

calponin homology and EB1 C-terminal domain characteristic of EB proteins are encoded in the *Drosophila* genome. CG32371 is expressed primarily in the testis and CG18190 in the ovary (Chintapalli et al., 2007), and neither gene has been associated with any phenotypes, so EB1 is most likely the major EB protein in neurons.
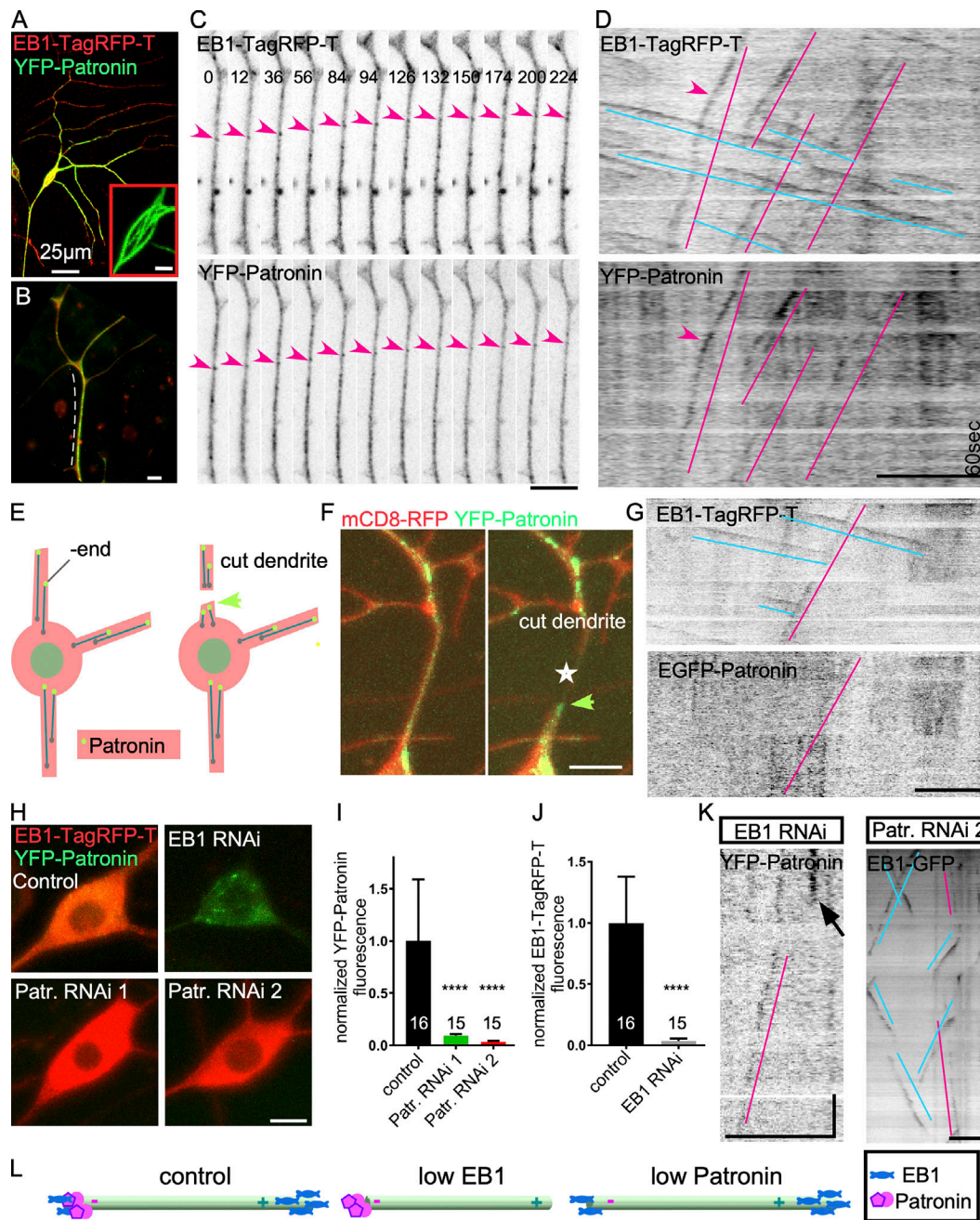
Figure 2. **EB1 and Patronin independently label the same growing microtubule minus ends. (A)** Representative image of a ddaE neuron expressing high levels of YFP-Patronin. EB1-TagRFP-T is coexpressed to show cell shape. Bar in inset, 5 µm. **(B–D)** Representative images and kymographs of a neuron with low expression levels of YFP-Patronin with EB1-TagRFP-T are shown. The dashed line in B indicates the region where C and D were generated. **(C)** Pink arrowhead points to a minus end colabeled with EB1-TagRFP-T and YFP-Patronin. Numbers on each image indicate the time in seconds. Bar, 5 µm. **(D)** Kymographs of EB1-TagRFP-T and YFP-Patronin. Minus ends are marked with pink lines and plus ends with turquoise lines. The pink arrowhead indicates the minus end shown in C. **(E)** Schematic diagram of predicted YFP-Patronin relocalization after dendrite severing. New microtubule minus ends generated by dendrite cut will recruit Patronin to only one side of the severed dendrite indicated by green arrowhead. **(F)** Representative images of YFP-Patronin accumulating at the distal end of a proximal dendrite segment after severing. mCD8-RFP was used as the cell shape marker. Star indicates the cutting site of comb dendrite. Green arrowhead indicates the relocalized YFP-Patronin. Bar, 5 µm. **(G)** Representative kymograph of EB1-TagRFP-T colocalized with EGFP-Patronin on a growing microtubule minus end. EGFP-Patronin was expressed from its own promotor. Horizontal bar, 5 µm. Vertical bar, 60 s. **(H)** Representative images of YFP-Patronin, EB1-TagRFP-T in the cell body of ddaE. All images were acquired with the same settings and processed in the same way. Bar, 5 µm. **(I and J)** Quantification of RNAi knockdown efficiency. FI of YFP-Patronin was measured in cell body of control, Patronin RNAi VDRC27654 (Patr. RNAi 1), or Patronin RNAi BL36659 (Patr. RNAi 2) neurons. FI of EB1-TagRFP-T was measured in cell body of control or EB1 RNAi VDRC24451 neurons. Raw FI was divided by the average FI of control neurons for normalization. Numbers on the graphs are the numbers of neurons imaged. ****, P < 0.0001 with Mann-Whitney U test. **(K)** Example kymographs of minus-ends labeling by YFP-Patronin or EB1-TagRFP-T together with EB1 or Patronin RNAi, respectively. Pink lines mark the minus end traces, and turquoise lines mark plus end traces. The black arrow indicates an immobile dot of YFP-Patronin. Horizontal bar, 5 µm. Vertical bar, 60 s. **(L)** Schematic diagram showing EB1 and Patronin colabel growing minus ends of microtubules and track them independently.

Two different Patronin RNAi transgenes were very effective at reducing levels of YFP-Patronin (Fig. 2, H and I; and see Fig. 4 A for target sites of the RNA hairpins). However, slow-moving EB1 dots were still observed in these backgrounds (Fig. 2 K). To confirm that endogenous Patronin was also eliminated under these conditions, we paired Patronin tagged at the endogenous locus with Venus (Nashchekin et al., 2016) with RNAi. Patronin-Venus signal was almost completely eliminated from the ddaE neuron expressing the RNAi hairpin, but not from neighboring neurons (Fig. S1, B and C). Thus, Patronin and EB1 can be effectively reduced by RNAi in neurons, and this reduction does not affect localization of the other protein to growing microtubule minus ends (Fig. 2 L).

Patronin is required for persistent minus end polymerization

In vitro CAMSAP2 and 3 as well as key domains of Patronin suppress minus end growth in a concentration-dependent manner (Hendershott and Vale, 2014; Jiang et al., 2014). We therefore asked whether Patronin also regulated minus end dynamics in neurons of intact animals. To analyze minus end polymerization properties, we acquired 20-min videos of ddaE neurons expressing EB1 fused to TagRFP-T, as this fluorophore is relatively resistant to photobleaching (Shaner et al., 2008). Minus ends were considered to be puncta that moved slower than 1.6 µm per minute, and are labeled in pink in example kymographs (Fig. 3 E). In control dendrites, minus ends polymerized for an average of 240 s (Fig. 3 C), with a quarter of minus end growth events lasting longer than 5 min (Fig. 3 D). Note that the average and number of long runs are underestimates as runs that began or ended outside the 20-min videos were excluded, and these likely are over-represented for long runs. In control neurons, most of the minus end growth was away from the cell body, as in the example shown in Fig. 3 F.

With Patronin knockdown, the duration of minus end polymerization decreased to ~80 and 60 s using two independent RNAi lines (Fig. 3 C). The persistent polymerization events over 5 min were almost completely abolished in these genotypes (Fig. 3 D). The growth length of microtubule minus ends was also significantly decreased from about 3 µm in control to about 1 µm (Fig. 3, B and E). In addition, the growth rate of microtubule minus ends was slightly increased with Patronin knockdown (Fig. 3 A). Similarly, mild overexpression of YFP-Patronin slowed minus end growth slightly compared with neurons in which minus end speed was measured with EB1-GFP or EGFP-Patronin (Fig. S2). Overall, these data support a role for Patronin in promoting extended periods of minus end growth, and slight suppression of growth rate.

As EB1 also labeled growing minus ends, we tested whether it was required for persistent minus end growth. Although EB1 RNAi effectively eliminated almost all protein (Fig. 2, H and J; and Fig. S1 D), it did not reduce the duration of minus end growth (Fig. S2, A and B). Its reduction did, however, slightly decrease minus end polymerization speed (Fig. S2 A), indicating that EB1 may promote subunit addition at the minus end.

To determine whether Patronin affected other parameters of neuronal microtubules, we examined stable microtubules and plus end growth. To monitor stable microtubules, we stained larval skins for the *Drosophila* MAP1B orthologue, futsch (Hummel et al., 2000). Futsch staining was slightly reduced, particularly in axons (Fig. S3, A and B), indicating that Patronin is likely required for overall neuronal microtubule stability. The behavior of plus ends was also altered when Patronin was reduced; polymerization speed was moderately increased (Fig. S3, C–E). The faster polymerization could be due to increased levels of free tubulin in neurons with less stable microtubules. Thus, reduction of Patronin has global effects on neuronal microtubules. However, the profound effect on minus end growth together with localization to minus ends suggests that its major role may be to promote minus end polymerization over extended time and distance (Fig. 3 G).

Patronin is required for minus-end-out microtubule polarity in dendrites

To determine whether minus end growth facilitated by Patronin might impact the overall organization of microtubules in dendrites, we assayed polarity in ddaE neurons with normal and reduced levels of Patronin. Dendrites of control ddaE neurons have around 90% minus-end-out microtubules (Stone et al., 2008; Fig. 4 B and Video 5). Knockdown of Patronin with three independent RNAi lines that target different regions of the transcript (Fig. 4 A) resulted in mixed polarity in the dorsal comb dendrite (Fig. 4, B and D; and Video 5). The polarity changes were stronger than those in kinesin-2 RNAi and mutant backgrounds (Mattie et al., 2010) and γtubulin mutant backgrounds (Nguyen et al., 2014). Despite the strong effect on dendritic polarity, no changes were seen in axons (Fig. 4 F).

To make sure that the polarity we detected using EB1 accurately reflected overall microtubule organization, we severed dendrites with a laser to produce new microtubule ends in stable regions of microtubules. All new plus ends moved toward the cell body as predicted by uniform minus-end-out polarity (Fig. S4, A and B). Similarly, Patronin accumulated only next to the cut site at the distal region of the dendrite still attached to the cell body (Fig. S4 C). Although there was no indication that polarity measured with EB1 did not capture overall microtubule polarity, we probed polarity of stable microtubule regions in control and low Patronin neurons using an assay based on microtubule steering (Mattie et al., 2010). At dendrite branch points, growing microtubules use the polarity of stable regions of microtubules to steer at the junction. When polarity is minus-end-out, this results in turning toward the cell body (Mattie et al., 2010; Fig. S4 D). If the stable regions used as tracks have mixed polarity, this will be reflected in growing microtubules turning in both directions. Indeed, in control neurons, almost all microtubule steered toward the cell body, while Patronin knockdown resulted in steering in both directions (Fig. S4 E), consistent with mixed polarity in these dendrites.

To confirm the RNAi results, we used two different mutant alleles of *Patronin*. *Patronin*[EY05252] contains a transposon insertion in its 5′ region (Fig. 4 A) and has been used previously as a hypomorphic allele (Nashchekin et al., 2016), and *Patronin*[k07433] has not been phenotypically characterized but contains a lethal transposon insertion in an intron of the *Patronin* gene (Bellen et al., 2004). In animals heterozygous for either allele,
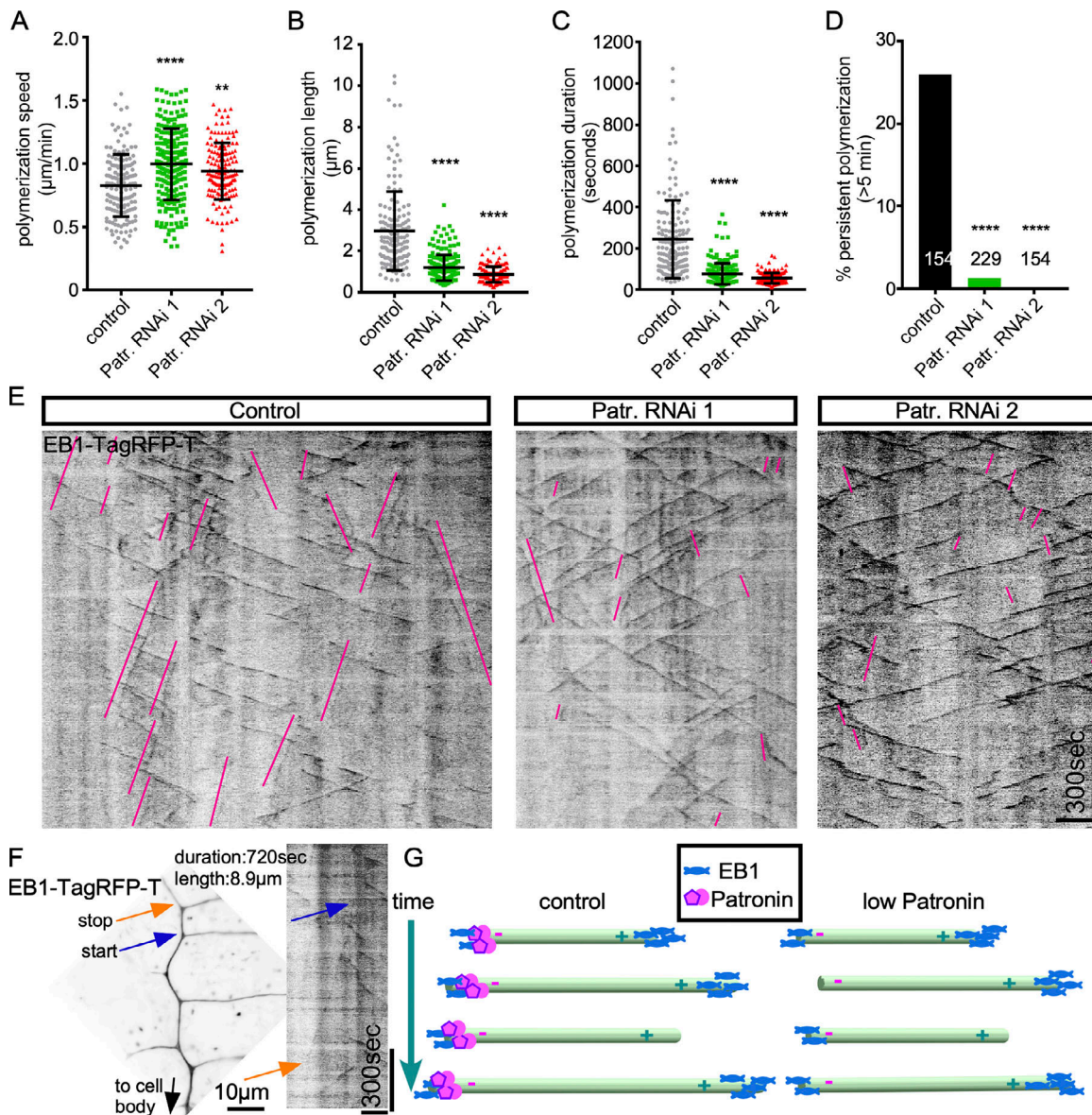
Figure 3. **Patronin is required for persistent minus end polymerization. (A–C)** Quantification of speed, polymerization length, and duration of minus ends of microtubules with control or Patronin RNAi. Sample sizes are 154 traces from 30 neurons for control RNAi, 229 traces from 21 neurons for Patronin RNAi 1, and 154 traces from 15 neurons for Patronin RNAi 2. **(A)** One-way ANOVA followed by Dunnett's multiple comparisons were used for statistics. **, $P < 0.01$; ****, $P < 0.0001$. **(B and C)** Kruskal–Wallis tests followed by Dunnett's multiple comparisons were performed because of non-Gaussian distribution of these data. ****, $P < 0.0001$. Mean and SD are shown with black lines. **(D)** Quantification of persistent minus end growth events. Minus ends that polymerized for >5 min were considered persistent growth. Numbers on the graph are the total numbers of traces collected. ****, $P < 0.0001$ with Fisher's exact test. **(E)** Representative kymographs of EB1-TagRFP-T with control or Patronin RNAi. Pink lines indicate minus ends. Horizontal bar, 5 µm. Vertical bar, 300 s. **(F)** Representative overview image of the comb dendrite from an EB1-TagRFP-T expressing class I ddaE neuron with control RNAi. Kymograph shows a representative persistent minus end growth event. Blue arrow points to the start and orange arrow to the end of the growth event in the overview and kymograph. **(G)** Schematic diagram showing Patronin is required for persistent minus end polymerization.

microtubule polarity remained unaffected (Fig. 4 C). Homozygous *Patronin*[EY05252] animals died early in development and so could not be analyzed for neuronal microtubule polarity. Homozygous *Patronin*[k07433] animals survived into larval stages and had normal microtubule orientation in ddaE neurons, indicating it is likely only a weak loss-of-function allele. Trans-heterozygous animals that contained one copy of each allele survived into larval stages, and dendritic microtubule polarity was mixed (Fig. 4, C and E). Similar results were obtained with *Patronin*[EY05252] crossed

in as the male or female parent (Fig. 4, C and E). In addition to polarity, we assayed minus end behavior in the mutant background. As in Patronin RNAi neurons, the duration and length of individual minus end growth events were dramatically reduced in the mutant background (Fig. S5, A–D). Since the mutant phenotypes were consistent with the RNAi ones, we used RNAi knockdown for the remaining analysis.

ddaE neurons have relatively simple dendrite arbors (Grueber et al., 2003b), with a right angle branching pattern
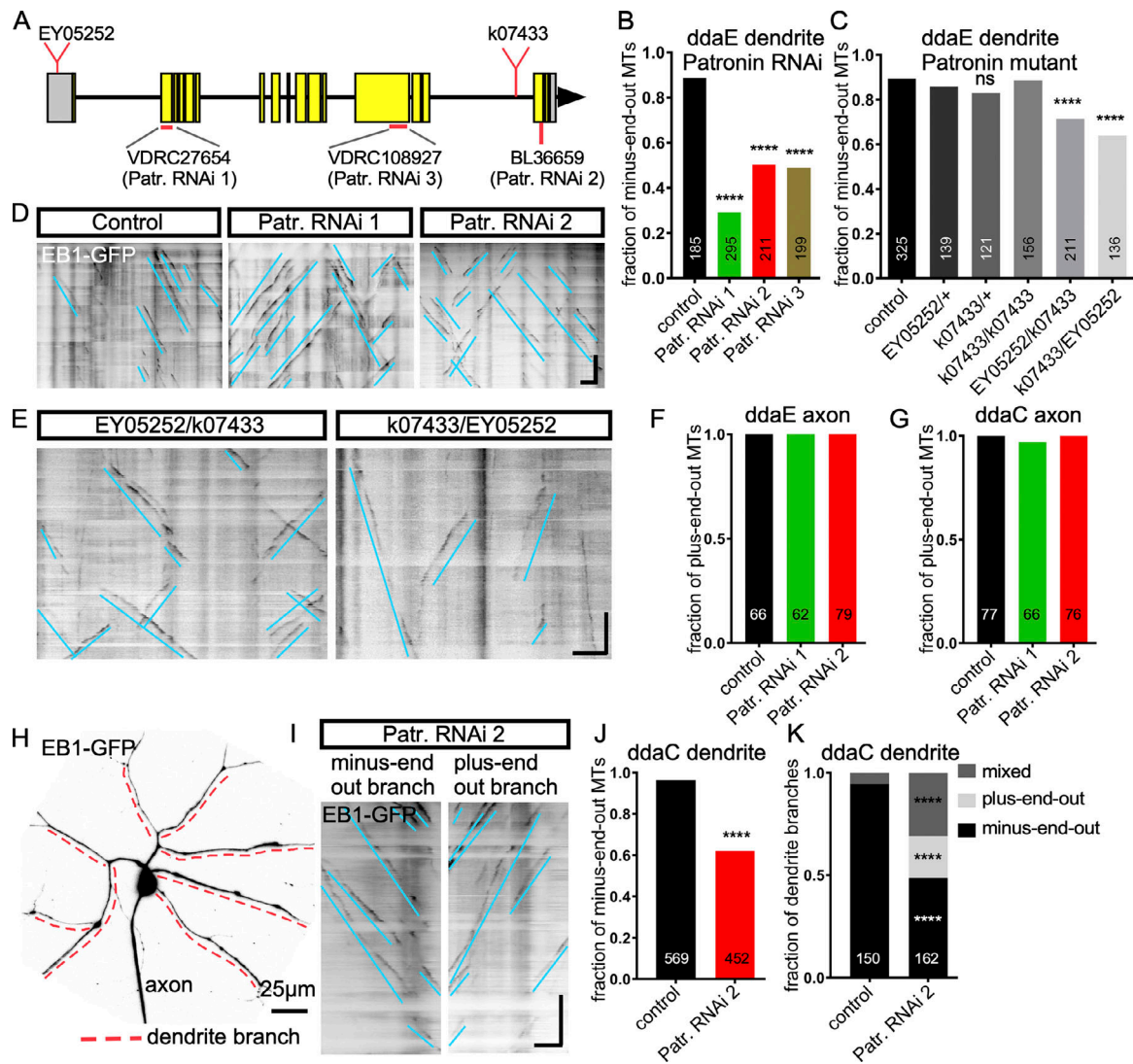
Figure 4. **Patronin is required for normal microtubule polarity in ddaE and ddaC neurons. (A)** Schematic representation of the *Patronin* gene region (based on RA isoform). Target sites for RNAi lines as well as transposon insertion sites are indicated. The two VDRC lines generate long hairpin RNAs, while the Bloomington (BL) line generates a small hairpin. **(B and C)** Quantification of dendrite microtubule polarity in ddaE neurons expressing EB1-GFP in genetic backgrounds that reduce Patronin. Numbers on the graph are the total numbers of comets collected from ≥10 neurons in each genotype. One neuron per animal was imaged. ns = not significant (P = 0.069); ****, P < 0.0001 with Fisher's exact test. **(D and E)** Representative kymographs of EB1-GFP with control RNAi, Patronin RNAi, or null/hypomorph mutants. Turquoise lines mark plus ends. Horizontal bar, 5 μm. Vertical bar, 60 s. **(F and G)** Quantification of axonal microtubule (MT) polarity in ddaE or ddaC neurons. Numbers on the graph are the total comet numbers collected from 14, 12, 20, 20, 10, and 17 neurons, respectively (left to right). **(H)** Representative image of a ddaC neuron expressing EB1-GFP. Dashed red lines indicate the major dendrite branches used for quantification in J and K. **(I)** Representative kymographs of EB1-GFP in a branch with minus-end-out microtubule polarity (left), or in a branch with plus-end-out microtubule polarity (right). Turquoise lines mark plus end traces. Horizontal bar, 5 μm. Vertical bar, 60 s. **(J)** Quantification of overall microtubule polarity in ddaC dendrites. Numbers are total comet numbers collected from 18 and 7 neurons, respectively. ****, P < 0.0001 with Fisher's exact test. **(K)** Quantification of ddaC major branches with plus-end-out, minus-end-out, or mixed microtubule polarity. Branches with >90% EB1-GFP comets moving toward the cell body are classified as minus-end-out branches. Dendrite branches with >90% EB1-GFP comets moving toward the distal tip are classified as plus-end-out branches. The rest are mixed polarity branches. Numbers on the graphs are the total major branches collected from 18 and 20 neurons. ****, P < 0.0001 with Fisher's exact test.

that makes them particularly susceptible to changes in microtubule polarity (Mattie et al., 2010). To determine whether Patronin was also important for microtubule polarity in neurons with more complex dendrite arbors with acute branching angles, we assayed phenotypes in class IV ddaC neurons with reduced Patronin function. Major dendrite branches (as indicated by red dotted lines in Fig. 4 H) were analyzed in these cells. In a control RNAi background, these

dendrite regions are predominantly minus-end-out (Fig. 4 J and Video 6). When we decreased Patronin levels using RNAi BL36659, overall microtubule polarity became mixed (Fig. 4 J and Video 6). Interestingly, in the majority of neurons tested, at least one of the major dendrite branches had reversed to predominantly plus-end-out polarity (Fig. 4, I and K). As in ddaE neurons, axonal microtubule polarity remained normal in ddaC cells (Fig. 4 G). Together, these data demonstrate that

Patronin regulates dendritic microtubule polarity in *Drosophila* sensory neurons.

To determine whether Patronin loss also affected the shape of the dendrite arbor, we used a membrane marker to label control and Patronin knockdown ddaC neurons. In RNAi experiments, Gal4 drivers that turn on as neurons are specified were used. This timing means that if Patronin protein is present in precursor cells, the phenotype may be masked in early cellular development. Control and Patronin dendrite arbors did not appear grossly different (Fig. S5 E). Indeed, the total length of the dendrite arbor was similar in both backgrounds (Fig. S5 F), as was branching pattern measured by Sholl analysis (Fig. S5 G). We also examined ddaE neuron shape in trans-heterozygous mutants. While the majority of cells looked normal, about a third had a misplaced axon and an unusual straight process (Fig. S5 H). Because no shape defects were seen with RNAi in the more elaborate ddaC neurons, we hypothesize that the ddaE phenotype may arise from a defect in mitosis or early specification of the ddaE neurons in mutant animals rather than a specific effect on dendrite outgrowth. Overall, the changes in microtubule polarity do not seem to directly result in shape changes.

DLK/JNK signaling is activated in neurons with downregulated Patronin, but is not responsible for changes in minus end growth or polarity in these cells

Before trying to understand how Patronin controlled dendritic microtubule polarity, we wished to eliminate indirect effects in response to stress induced by reduction of a key microtubule regulator. Cytoskeletal disruption or changes in axon transport can cause a neuronal stress response that alters microtubule dynamics through transcription factors fos or FoxO (Massaro et al., 2009; Chen et al., 2012; Nechipurenko and Broihier, 2012; Valakh et al., 2013). Some of these stress responses are mediated by DLK/JNK signaling (Massaro et al., 2009; Chen et al., 2012; Valakh et al., 2013; Marcette et al., 2014) and overlap with signaling initiated by axon severing (Chen et al., 2012). After axon injury, DLK acts through JNK to turn on transcription through fos, and the MAPK phosphatase puc can be used as a reporter for this stress pathway (Xiong et al., 2010; Stone et al., 2014). Neuronal stress can also result in increased microtubule dynamics; in *Drosophila* and mammalian models of neurodegeneration, as well as after axon severing, more growing microtubule plus ends per unit length are observed (Chen et al., 2012; Kleele et al., 2014). Patronin loss has been shown to activate DLK signaling in *C. elegans* (Marcette et al., 2014), so we wished to determine whether this kinase pathway was also activated here.

To determine whether reduced Patronin activated a neuronal stress response, we used puc-GFP as a reporter of JNK/fos activation. In control neurons, low levels of puc-GFP were seen in the nucleus of the ddaE neuron (Fig. 5, A and B). Both Patronin RNAi lines resulted in elevated puc-GFP nuclear signal (Fig. 5, A and B). Consistent with activation of a stress response, microtubule dynamics was also elevated (Fig. 5 C). Thus, knockdown of Patronin initiated a stress response similar to that induced by axon injury. As this type of stress response can dramatically affect microtubules (Chen et al., 2012), we wished to separate secondary stress phenotypes from phenotypes that might be directly due to loss of Patronin.

To dampen the stress response, we fed animals two different inhibitors of JNK and DLK and chose concentrations that resulted in puc-GFP signal similar to control levels in Patronin RNAi neurons (Fig. 5, A and B). SP600125 is a JNK inhibitor (Bennett et al., 2001) that has been broadly used, including in *Drosophila* larvae (Chen et al., 2010). GNE-3511 is a more recently generated DLK inhibitor (Patel et al., 2015). Treatment with GNE-3511 seemed to partially reduce microtubule dynamics in both RNAi backgrounds, and SP600125 results were ambiguous in this assay (Fig. 5 C), consistent with it being slightly less effective at eliminating the puc-GFP signal. Microtubule polarity remained mixed in Patronin RNAi neurons exposed to either drug (Fig. 5, D and E). Like polarity, the reduction in persistent minus end growth was not suppressed by the DLK inhibitor (Fig. 5, F and G). We conclude that reduction of Patronin induces a DLK- and JNK-dependent transcriptional stress response and that increased microtubule dynamics may be secondary to this stress response (Fig. 5 H). In contrast, the effect of Patronin on microtubule polarity and persistent microtubule minus end growth does not depend on DLK and JNK signaling and is therefore likely due to direct function of Patronin on microtubules (Fig. 5 H).

Minus end growth populates dendrite tips with minus-end-out microtubules

So far, the data suggested that Patronin promotes individual bouts of minus end growth that can continue for minutes and extend the microtubule over 10 µm. In addition, Patronin function was required for the minus-end-out arrangement of dendritic microtubules. γTubulin concentrates at dendrite branch points and is important for the minus-end-out organization of dendritic microtubules (Fig. 6 A; Nguyen et al., 2014). However, most dendrite tips do not contain obvious patches of γtubulin (Fig. 6 A). We therefore hypothesized that minus end growth mediated by Patronin could populate the tips of dendrites beyond branch points with minus-end-out microtubules (Fig. 6 B).

To determine whether Patronin might facilitate growth of minus ends toward dendrite tips, we analyzed microtubule polarity in terminal branches of the ddaE neuron with different levels of Patronin (Fig. 6 C). ddaE dendrite tips have mixed rather than minus-end-out polarity (Fig. 6, D and E; Stone et al., 2008). With Patronin knockdown, the proportion of minus-end-out microtubules in terminal dendrites was reduced (Fig. 6, D and E), and the number of minus ends in the same region was also lower (Fig. 6 E). The effect of Patronin overexpression was also analyzed. Patronin tagged with Venus at the endogenous locus (Nashchekin et al., 2016) was used as a control and to estimate expression levels of EGFP-Patronin (Takeda et al., 2018) and YFP-Patronin. Taking into account the two endogenous copies of untagged Patronin, EGFP-Patronin was estimated to mildly increase overall expression, and YFP-Patronin was estimated to result in about twofold more total Patronin in ddaE (Fig. 6 G and Materials and methods). As expected, the polarity
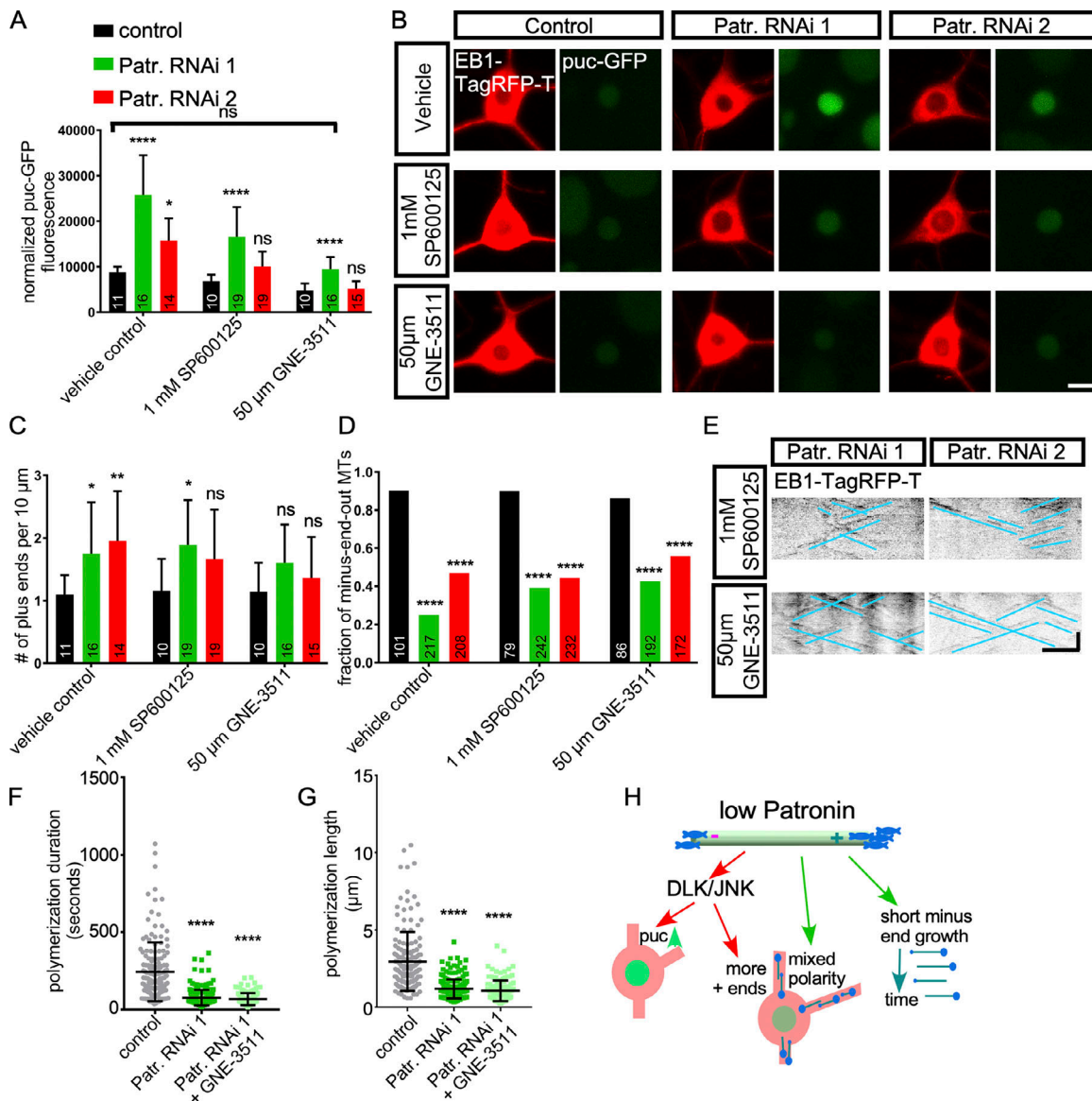
Feng et al.
Microtubule minus ends grow into dendrites

Journal of Cell Biology
https://doi.org/10.1083/jcb.201810155

2317

Figure 5. **Patronin knockdown activates DLK/JNK signaling, but only a subset of phenotypes depends on DLK/JNK. (A–D)** Quantification of FI of puc-GFP reporter and microtubule dynamics with drug treatments. Numbers on the graph are numbers of neurons quantified. The same neurons were used to measure puc-GFP levels, microtubule dynamics, and polarity. *, P < 0.05; **, P < 0.01; ****, P < 0.0001 with one-way ANOVA followed by Dunnett's multiple comparison. Statistical tests were performed for each drug treatment group, except for the comparison between control RNAi with vehicle control and Patronin RNAi 1 with GNE-3511 treatment for puc-GFP reporter, which was done by t test. **(B)** Representative images of puc-GFP reporter coexpressed with EB1-TagRFP-T. Bar, 5 µm. **(D)** Numbers on the graph are the total comet numbers collected from each group. ****, P < 0.0001 with Fisher's exact test. **(E)** Representative kymographs of EB1-TagRFP-T with drug treatments. Turquoise lines mark plus ends. Horizontal bar, 5 µm. Vertical bar, 60 s. **(F and G)** Quantification of minus end polymerization duration and length with drug treatment. Note that the control RNAi and Patronin RNAi 1 data have been shown in Fig. 3, B and C, and are shown again here for comparison. In the drug treatment group, 135 traces were collected from 18 neurons. Kruskal–Wallis tests followed by Dunnett's multiple comparisons were performed because of non-Gaussian distribution of these data. ****, P < 0.0001. **(H)** Schematic diagram showing the effects of Patronin knockdown. Note that short minus end growth phenotype and mixed polarity are not secondary to activated DLK/JNK signaling.

in Patronin-Venus expressing neurons was very similar to neurons expressing only EB1-GFP (Fig. 6, E, F, and H). However, even mild overexpression of Patronin resulted in a dramatic increase in minus-end-out microtubules in dendrite tips (Fig. 6, F and H), suggesting that Patronin levels normally limit minus-end-out polarity microtubules in this part of the cell.

Eventually microtubules extending from their minus end are expected to reach the end of the dendrite. To determine their fate at the tip, we visualized growing minus ends by coexpressing

EB1-TagRFP-T and YFP-Patronin and acquired videos of distal dendrites. Out of 19 minus ends that reached the end of a dendrite during imaging, 13 minus ends depolymerized immediately after reaching the tip, while 6 paused for ≥50 s at the tip (Fig. 6, I and J). This pausing behavior is reminiscent of the behavior of EB1-coated plus ends that encounter the cell cortex (Mimori-Kiyosue et al., 2005). Together, these data strongly support the idea that Patronin helps populate distal regions of dendrites with minus-end-out microtubules by promoting growth of the minus end.
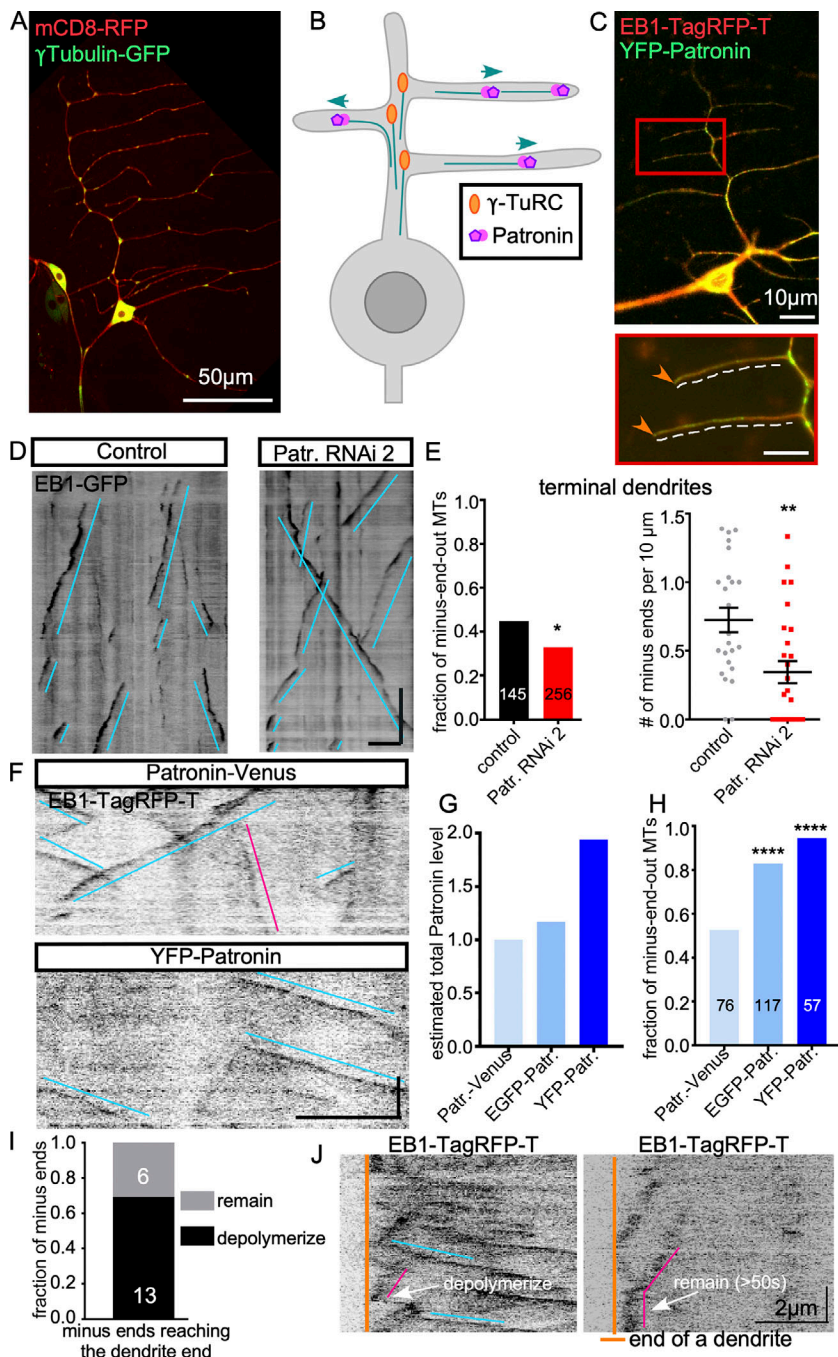
Figure 6. **Patronin is necessary and sufficient to add minus-end-out microtubules to terminal dendrites.** **(A)** Representative image of γtubulin-GFP coexpressed with mCD8-RFP in class I neurons. Note that γtubulin is concentrated at branch points. **(B)** Schematic diagram showing the hypothesis that the γtubulin ring complex (γ-TuRC) and Patronin both contribute to dendritic microtubule polarity, and that Patronin is particularly important beyond branch points. **(C)** Representative overview image of a ddaE neuron expressing EB1-TagRFP-T and YFP-Patronin. Bar, 10 μm. Red rectangular region was enlarged to show two secondary dendrites. White dashed lines mark examples of terminal dendrite branches used for analyzing microtubule polarity here. Dendrite tips are indicated with orange arrowheads. Bar, 5 μm. **(D)** Representative kymographs showing microtubule polarity of terminal dendrites of control or Patronin RNAi neurons. Turquoise lines indicate plus ends. Horizontal bar, 5 μm. Vertical bar, 60 s. **(E)** Quantification of microtubule polarity in terminal dendrites of ddaE neurons is shown in the left graph. Numbers on the graph are total comet numbers collected from 18 and 23 neurons. *, P < 0.05 with Fisher's exact test. Quantification of overall density of minus ends is shown in the right graph. Data were collected from 24 and 27 terminal dendrites from 18 and 23 neurons, respectively. **, P < 0.01 with Mann–Whitney U test. **(F)** Example kymographs of EB1-TagRFP-T showing microtubule polarity in terminal dendrites of ddaE neurons expressing CRISPR-tagged Patronin-Venus or UAS-YFP-Patronin. Turquoise lines indicate plus ends. Pink line indicates minus ends. Horizontal bar, 5 μm. Vertical bar, 60 s. **(G)** FI-based estimation of total Patronin protein levels when crossing with tagged Patronin fly lines. FIs were measured from 12 neurons of each genotype. Mean FI was used for normalization and plotted in the graph. See Materials and methods for information about how FI was normalized across fluorophores. **(H)** Quantification of microtubule polarity in terminal dendrites. Numbers on the graph are total comet numbers collected from 15, 15, and 14 neurons. ****, P < 0.0001 with Fisher's exact test. **(I)** Quantification of events occurring when growing minus ends reach the dendrite tip. Numbers on the graph are the numbers of minus ends encountering the end. Data were collected from 16 neurons. Minus ends were classified as remaining at the tip if they persisted there for ≥50 s. These data were collected from cells expressing YFP-Patronin with EB1-TagRFP-T, so the number of minus ends reaching tips is higher than in control neurons because more minus-end-out microtubules are present in terminal dendrites when extra Patronin is present. **(J)** Representative kymographs of EB1-TagRFP-T with mild overexpression of YFP-Patronin. Only EB1-TagRFP-T traces are shown. Solid orange lines in kymograph indicate the tip of the dendrite. Minus ends are marked with pink lines and plus ends with turquoise lines. Depolymerized and persistent events are shown. Horizontal bar, 2 μm. Vertical bar, 60 s.

Microtubule minus ends grow into dendrites during development

Based on the ability of minus end polymerization to help minus-end-out microtubules grow to dendrite tips of mature neurons, we hypothesized that a similar process might take place during development to establish polarity in dendrites. To track

microtubule organization during early dendrite development, we expressed EB1-GFP using the 1407-Gal4 (also known as insc-Gal4) driver, which is active in embryonic neuroblasts (Luo et al., 1994). Live imaging of microtubule dynamics in developing dendritic arborization neurons was performed in whole-mounted embryos. Developing neurons were categorized into three main

stages based on their dendrite morphology. Stage 0 neurons extended short unbranched processes that were populated by microtubules growing from the cell body with plus ends leading and thus had primarily plus-end-out polarity (Fig. 7, A and B; and Video 7). Stage 1–4 dendrites have been described previously and have mixed microtubule polarity (Hill et al., 2012; Fig. 7, A and B; and Video 7). In these stages, minus ends of microtubules were observed growing into dendrites (Fig. 7 C). At later stages of dendrite development, the arbor was branched, and polarity became predominantly minus-end-out (Fig. 7, A and B; and Video 7). When Patronin levels were reduced with RNAi, overall polarity failed to convert to minus-end-out during dendrite development, and microtubule orientation remained mixed late in embryogenesis (Fig. 7, B and D; and Video 8). Together, these data demonstrate that Patronin is required to establish minus-end-out microtubule polarity during dendrite development, most likely by promoting minus end growth into dendrites.

Patronin is required to generate minus-end-out microtubule arrays during dendrite regeneration

We have previously shown that after complete dendrite removal, *Drosophila* dendritic arborization neurons can grow a new dendrite arbor (Stone et al., 2014). The capacity to regenerate dendrites is particularly striking in ddaC neurons, which have large complex arbors. Regeneration is well underway by 24 h after dendrite removal, and the new arbor covers its previous territory by 96 h (Stone et al., 2014). Based on the importance of Patronin in populating dendrites with minus-end-out microtubules during development, we hypothesized that it might also play a role during regeneration. Indeed, RNAi knockdown of Patronin in ddaC neurons reduced the amount of dendrite outgrowth observed 24 h after dendrites were removed with laser microsurgery (Fig. 8, A and B).

During dendrite regeneration, microtubules reset their polarity de novo, and gradually reorganize from mixed orientation to uniform minus-end-out polarity (Stone et al., 2014; Fig. 8 D). To determine whether minus ends were actively growing outward in dendrites at early time points during regeneration, we imaged growing minus ends colabeled with EB1-TagRFP-T and YFP-Patronin. 24 h after dendrite removal, minus ends were readily observed extending into new dendrites (Fig. 8 C and Video 9). To determine whether minus end outgrowth might be functionally important in establishing microtubule polarity in this context, we knocked down Patronin in neurons expressing EB1-GFP and performed dendrite injury. In neurons with reduced Patronin, very few minus-end-out microtubules entered regenerating dendrites, and microtubule polarity remained over 75% plus-end-out at 16 h, 24 h, and 48 h after dendrite injury (Fig. 8, C–E; and Video 10). These data suggest that Patronin facilitates growth of minus-end-out microtubules in regenerating dendrites and that this process is essential for dendrite regrowth and reestablishment of minus-end-out polarity.

Discussion

In contrast to the traditional view that microtubule plus end growth is exclusively responsible for extending microtubules,

we found that in neurons, minus ends undergo extensive growth, with some individual runs lasting ≥10 min. Surprisingly, Patronin facilitates the persistent slow growth of minus ends, allowing them to elongate microns in single growth runs. Moreover, this minus end growth has critical functions in organizing the neuronal microtubule cytoskeleton, including populating growing dendrites and distal regions of mature dendrites with minus-end-out microtubules.

Neuronal DLK/JNK stress signaling is a common response to reduced Patronin in *C. elegans* (Marcette et al., 2014) and *Drosophila* (Fig. 5). As this signaling is responsible for some of the phenotypes observed in both systems, it will be important to determine whether any of the phenotypes that have been described in mammalian neurons with reduced CAMSAP2 are downstream of DLK or JNK. Changes in microtubule dynamics are a key output of neuronal stress from expression of proteins that cause neurodegeneration in flies (Chen et al., 2012) and mammals (Kleele et al., 2014), so some of the phenotypes attributed to direct function of CAMSAP2 could be secondary to stress. Our data suggest that in *Drosophila*, Patronin directly regulates minus end extension and microtubule polarity, but that changes in microtubule dynamics may be secondary to stress signaling.

Persistent minus end growth facilitated by Patronin could be an evolutionary innovation in animals like *Drosophila* that have mostly minus-end-out dendrites. However, we were also able to visualize growing minus ends that behaved similarly to the ones in *Drosophila* dendrites in plus-end-out zebrafish sensory endings. If this phenomenon is widespread across evolutionarily distant taxa, then why has it not previously been reported? EB proteins have been used to visualize microtubule plus end growth in neurons since 2003 (Stepanova et al., 2003), but slow-moving dots have not been noted before in neurons. One reason for this is likely improvements in sensitivity and signal-to-noise detection in microscopes used for live imaging. However, upon close inspection, there seem to be occasional minus ends in published EB data; for example, slow dim EB structures are present in kymographs from *Drosophila* (Fig. 1 A in Ori-McKenney et al., 2012) and mammalian neurons (Figs. 1i and 7b in Sánchez-Huertas et al., 2016; Fig. 4 A in Muhia et al., 2016; Fig. 1 F in Stepanova et al., 2010). In the future, it will be important to investigate behavior of microtubule minus ends in neurons from other species in detail to determine whether minus ends grow for long periods and over substantial distances.

It is particularly interesting to compare minus end growth across species because of the expansion of the Patronin/CAMSAP family in vertebrates. In zebrafish, we were able to observe clear minus end growth, but do not yet know which of the five CAMSAPs (two each of CAMSAP1 and 2 and one CAMSAP3; King et al., 2014) in fish might be present at these growing minus ends. In contrast to CAMSAP2 and 3, which suppress minus end growth, CAMSAP1 tracks minus ends as they grow (Hendershott and Vale, 2014; Jiang et al., 2014), so it is a good candidate. However, knockdown of CAMSAP1 has not been associated with changes in microtubule behavior in immortalized cell cultures (Jiang et al., 2014) and was not detected in neurons in the hippocampus (Yau et al., 2014). In contrast, CAMSAP2 knockdown
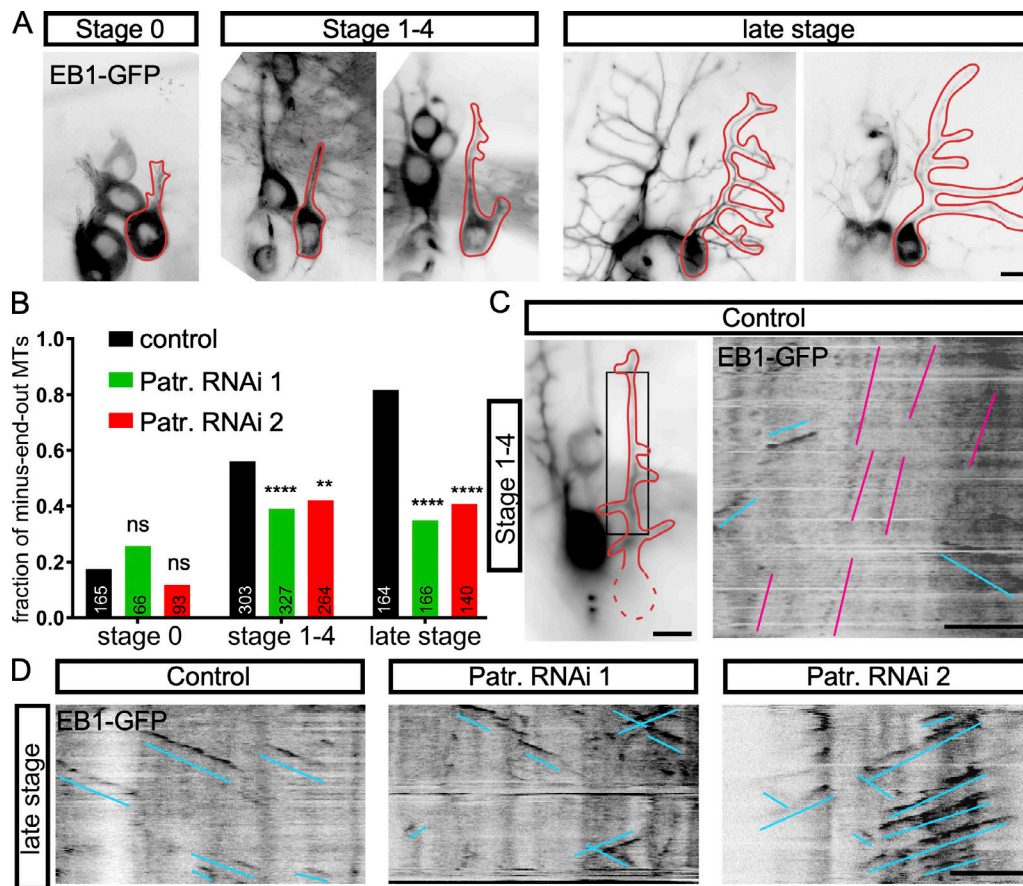
Figure 7. **Patronin is required to establish minus-end-out microtubule polarity during dendrite development. (A)** Representative images of ddaE neuron embryonic dendrite development. Red line outlines the cell body and dendrite arbor. Axons extend down in all panels. Bar, 5 µm. **(B)** Quantification of microtubule polarity during development. Numbers on the graph are the total comet numbers collected from 10, 4, 7, 21, 25, 22, 17, 12, and 11 neurons from left to right. **, P < 0.01; ****, P < 0.0001. **(C)** Representative image and kymograph of EB1-GFP–labeled minus ends entering developing dendrite of ddaE neuron. On the left is the overview of a stage 1–4 ddaE neuron outlined in red. The black box indicates the region where the kymograph on the right was generated. Turquoise lines mark plus ends, and pink lines mark minus ends. Horizontal bar, 5 µm. Vertical bar, 60 s. **(D)** Representative kymographs of EB1-GFP from late-stage ddaE neurons expressing the indicated RNAi hairpins. Cyan lines mark plus ends. Horizontal bar, 5 µm. Vertical bar, 60 s.

has dramatic effects on microtubule stability in immortalized cells (Jiang et al., 2014) and neurons (Yau et al., 2014), so it is an open question what family member might be present on the growing minus ends we tracked in zebrafish sensory neurons and how different types of CAMSAPs might cooperate or compete with one another.

The finding that *Drosophila* Patronin facilitates, rather than reduces, minus end growth in neurons is surprising in light of its previous characterization. Rather than tracking growing minus ends like CAMSAP1, it is thought to dampen minus end growth like CAMSAP2 and 3 (Hendershott and Vale, 2014). One possible explanation for this discrepancy between Patronin behavior in vitro (Hendershott and Vale, 2014) and in neurons is that in specific cell types or contexts, its behavior at minus ends could be regulated. In vitro, the coiled coil domain of Patronin tracks dynamic minus ends, and when the neighboring CKK domain is added, the behavior switches to growth suppression (Hendershott and Vale, 2014). In vivo, perhaps the effect of the CKK domain is modulated to uncover the minus end growth tracking ability of the coiled coil domain.

The neuronal phenotypes from reduction of Patronin are consistent with a role in minus end growth, and we propose that extended periods of minus end growth allow minus-end-out microtubules to grow into dendrites. Consistent with this idea, Patronin reduction resulted in fewer minus-end-out microtubules in distal regions of mature dendrites as well as in developing and regenerating dendrites. However, other mechanisms likely work in parallel with minus end growth to populate dendrites with microtubules.

Sliding of minus-end-out microtubules along plus-end-out ones by kinesin-6 motors was the mechanism first proposed to populate dendrites with minus-end-out microtubules in mixed polarity mammalian neurons (Sharp et al., 1997; Yu et al., 1997, 2000), and the function of kinesin-6 has been confirmed more recently with newer methods (Lin et al., 2012). In *Drosophila*, these motors could play a role in dendritic microtubule organization early in development when microtubules in dendrites are mixed, but it is harder to imagine how they might function in mature minus-end-out dendrites. Analysis of Pavarotti, one of the *Drosophila* kinesin-6 motors, confirms that it is unlikely to play a major role in polarity of mature dendrites, and actually
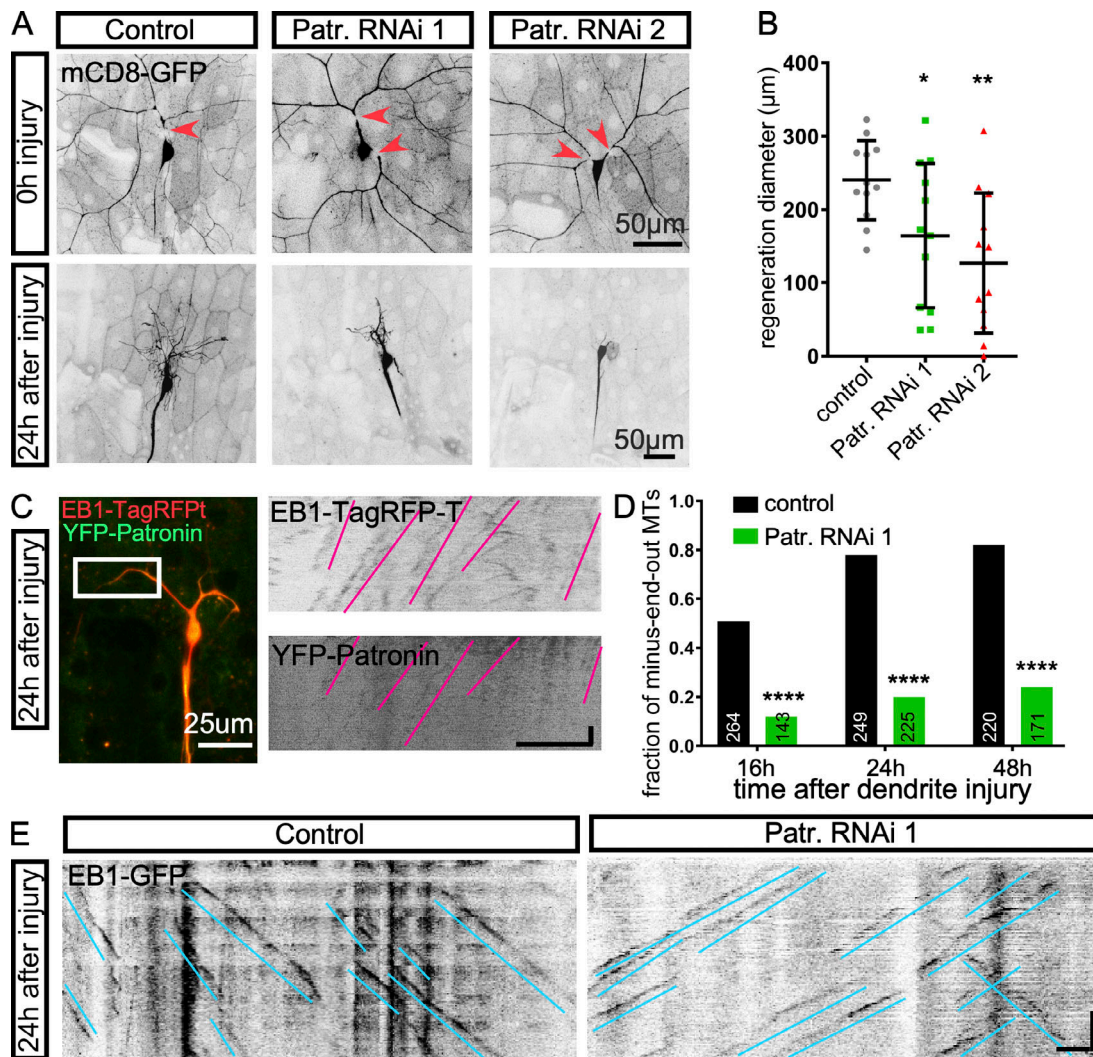
Figure 8. **Patronin function during dendrite regeneration is required for outgrowth and establishment of microtubule polarity. (A)** Representative images of ddaC neurons expressing mCD8-GFP immediately after or 24 h after dendrite severing. Bar, 50 µm. Red arrowheads indicate cut sites. **(B)** Quantification of dendrite regeneration. 24 h after dendrite injury, the greatest diameter of the regenerated dendrite arbor was measured. Averages and SDs are shown as well as data from each neuron. *, P < 0.05; **, P < 0.01 with a t test. **(C)** Representative image and kymographs or EB1-TagRFP-T and YFP-Patronin in regenerating dendrites. Left: Overview of merged channels showing regeneration 24 h after dendrite injury. Bar, 25 µm. Right: Kymographs showing minus ends labeled by EB1-TagRFP-T and YFP-Patronin growing toward the dendrite tip. Pink lines mark the minus ends. Horizontal bar, 5 µm. Vertical bar, 60 s. **(D)** Quantification of microtubule polarity during dendrite regeneration. Microtubule polarity was measured at 16, 24, or 48 h after dendrite injury in regenerating ddaC dendrites. Neurons expressed EB1-GFP as well as the indicated RNAi hairpins. Numbers on the graph are the total comet numbers collected from 15, 8, 14, 12, 7, and 9 neurons from left to right. ****, P < 0.0001 with Fisher's exact test. **(E)** Representative kymographs of EB1-GFP in regenerating dendrite at 24 h after dendrite injury. Turquoise lines mark plus ends. Horizontal bar, 5 µm. Vertical bar, 60 s.

reduces sliding of microtubules by kinesin-1 into developing axons (Del Castillo et al., 2015).

Local nucleation of microtubules in dendrites can also help populate dendrites with microtubules and, in contrast to sliding, has been shown to be important in *Drosophila* (Ori-McKenney et al., 2012; Nguyen et al., 2014) and *C. elegans* (Harterink et al., 2018). In mammalian neurons, noncentrosomal microtubule nucleation also predominates and is known to be critical for axon growth and microtubule organization (Stiess et al., 2010; Sánchez-Huertas et al., 2016), though the localization and role of nucleation sites in dendrites has not been detailed so far. During *C. elegans* development, microtubule nucleation operates in parallel to minus end regulation by Patronin (Wang et al., 2015),

and both types of minus end regulation may cooccur broadly in different cell types and species. In different contexts, nucleation or Patronin may vary in relative importance. For example, during initial dendrite outgrowth, we did not observe strong morphological defects with Patronin knockdown, but during regeneration, dendrite growth was strongly perturbed. While differences in RNAi knockdown could account for the phenotypic differences, it is also possible that nucleation can compensate more completely for Patronin reduction in development compared with regeneration.

Overall, we have demonstrated that, rather than existing as static structures, microtubule minus ends can grow in *Drosophila* and zebrafish neurons. Minus end growth is slow, but

persistent, and up to 10 µm can be added in a single episode of growth. While both EB proteins and Patronin can bind to minus ends, they do so independently, and Patronin is critical for extended stretches of minus end growth. Without Patronin-mediated minus end growth, minus-end-out microtubules were reduced in dendrite tips and developing dendrites. Moreover, extra Patronin was sufficient to convert dendrite tips from mixed polarity to minus-end-out. Dendrite regeneration was particularly sensitive to Patronin reduction. We conclude that minus end microtubule growth is likely to be broadly important in helping minus-end-out microtubules reach cellular regions that are distal to nucleation sites.

Materials and methods

Drosophila and zebrafish maintenance
Drosophila
Droshila were maintained on cornmeal fly food at 20 or 25°C. 1 liter of fly food contains 4.5 g of agar, 25.9 g of sucrose, 51.7 g of dextrose, 15.5 g of yeast, 4 ml of propionic acid, 6 ml of tegosept, and 85.8 g of cornmeal. For most experiments, embryos were collected on 35-mm plates filled with fly food for 24 h, and then caps were aged at 25°C for 3 d. To study developing neurons, fly embryos were collected for 24 h at 25°C on apple juice agar caps supplied with yeast paste. One neuron was imaged per animal. Sex of larvae was not differentiated in this study.

Danio rerio
Zebrafish were maintained in an Aquaneeering fish habitat, at a density of three fish per liter, sex separated, with weekly mating intervals. Adult fish were fed brine shrimp twice daily and were kept on a 14-h-light/10-h-dark cycle at 28.5°C at pH 7.5. To generate larvae for experiments, embryos were raised in glass bowls at 28.5°C in 1× Blue Water (0.6 g/l Instant Ocean salt mix and 0.01 mg/l methylene blue), and imaged before requiring food. Sex was not determined as fish have nonchromosomal sex selection that does not take place by the time point of 72 h postfertilization (hpf). 50% water exchanges were performed with fresh 28.5°C Blue Water every day. All zebrafish experiments were performed after receiving approval from the Institutional Animal Care and Use Committee, and guidelines on euthanasia and pain management were followed.

Plasmid construction and Drosophila and zebrafish strains
Drosophila strains were obtained from both the Bloomington Drosophila Stock Center (BDSC) and the Vienna Drosophila Resource Center (VDRC). Information about the strains including identifiers is contained in Table S1.

To generate YFP-tagged Patronin, we first amplified the coding sequence of Patronin from cDNA clone AT18914 (*Drosophila* Genomics Resource Center collection) using primers: forward, 5′-ATGGCGCGCCAATGGATGTCGAAACACAGGAA-3′; reverse, 5′-ATAGGTACCTTAGATTACAAGCGCCATGTCT-3′. An AscI digestion site was included in the forward primer and a KpnI one in the reverse primer for cloning purposes. The coding region was then inserted to multiple cloning sites of a modified pUAST vector with three copies of YFP preinserted at the 5′ side of the multiple cloning site (Rolls et al., 2007). Next, this pUAST-3xYFP-Patronin plasmid was injected into fly embryos by BestGene Inc. Standard screening and mapping processes were applied, and fly lines expressing high or low levels of UAS-3xYFP-Patronin (denoted YFP-Patronin) were used.

To generate TagRFP-T–tagged EB1, we first amplified the coding sequence of TagRFP-T from TagRFP-T-EEA1 plasmid (42635; Addgene). The start codon was changed to GTG, and 3× stop codon of TAGTAATGA was added to the 3′ end using primers: forward, 5′-TATGGCCGGCCTGCTAGCGGTAGTGGAGGT GTGGTGTCTAAGGGCGAAGAG-3′; reverse, 5′-CTTCTAGATCAT TACTACTTGTACAGCTCGTCCATGCC-3′. An FseI site was included in the forward primer and XbaI to the reverse primer for cloning. Previously described pUAST-EB1-tdimer12 (Mattie et al., 2010) plasmid that contains the *Drosophila* EB1 coding sequence upstream of the tdimer12 coding sequence under control of a 5X UAS sequence was used as the backbone, and the tdimer12 coding sequence was replaced with that of TagRFP-T to make pUAST-EB1-TagRFP-T plasmids. Fly lines were generated as described above. Lines that resulted sharp EB1 comets when crossed with our standard Gal4 drivers were used in this study.

Tester lines used in study included (1) UAS-dicer2; 221-Gal4, UAS-EB1-GFP/TM6, (2) 221-Gal4, UAS-dicer2, UAS-EB1-TagRFP-T/TM6, (3) UAS-YFP-Patronin/CyO-pAct-GFP; 221-Gal4, UAS-dicer2, UAS-EB1-TagRFP-T, (4) 221-Gal4, UAS-dicer2, UAS-EB1-TagRFP-T, puc-GFP/TM6, (5) 477 Gal4, UAS-EB1-GFP/CyO; UAS-dicer2, (6) 1407-Gal4, UAS-EB1-GFP; UAS-dicer2, and (7) UAS-dicer2; ppk-Gal4, UAS-mCD8-GFP. Flies from tester lines were crossed with RNAi animals to generate larvae for experiments. UAS-dicer2 was included in every RNAi experiment to generate greater knockdown efficiency (Dietzl et al., 2007). 221-Gal4 was used to drive transgene expression in class I dorsal dendritic arborization ddaD and ddaE neurons (Grueber et al., 2003a), but only ddaE neurons were used for quantification. 477-Gal4 or ppk-Gal4 was used for class IV ddaC neuron expression (Grueber et al., 2003b). 1407-Gal4 (Luo et al., 1994) drove expression of transgenes in a cluster of neurons including ddaE in embryonic and early larval stages. EB1-GFP or EB1-TagRFP-T was used to study microtubule dynamics. mCD8-GFP was used as a cell shape marker. Patronin mutants *EY05252* and *k07433* were rebalanced with CyO-pAct-GFP balancer so that mutant larvae could be identified. To control for any maternal effects, we used female flies from *EY05252* (marked as *k07433/EY05252*) as well as female flies from *k07433* (marked as *EY05252/k07433*) to generate trans-heterozygous mutant animals. γTubulin-37C RNAi was used as control for RNAi experiments as γTubulin-37C is a maternal gene that is not expressed in somatic tissues (Wiese, 2008). *yw* was used as the control background for *Patronin* mutant experiments. Many fly lines used in this study were acquired from the BDSC or the VDRC. Detailed fly line information can be found in Table S1.

To generate the pEX_P2X3.E1B:LexA-VP16.Sv40.4XLex-Aop.E1B:EB3-GFP.Sv40 plasmid that was used to mark growing microtubule ends in zebrafish, we performed a Gateway LR reaction with the following entry vectors: p5E: P2X3 enhancer fragment (Palanca et al., 2013); pME: E1B.LexA-VP16.Sv40.4xLexAop.E1B; p3E: EB3-GFP. p3E: EB3-GFP was

generated by PCR amplification from pCSEB3-GFP containing the human EB3 protein tagged with GFP (Distel et al., 2010). PCR amplification was performed with nonpriming additions of attB sites for use with a Gateway BP reaction with a 3′ DONR vector (primer sequences: forward, 5′-GGGGACAGCTTTCTTGTACAA AGTGGCTGCCACCATGGCCGTCAAT-3′; reverse, 5′-GGGGAC AACTTTGTATAATAAAGTTGTTTACTTGTACAGCTCGTCCAT GC-3′). The destination vector used for the LR reaction was pDestTol2pA2. The final product was coinjected with tol2 mRNA into zebrafish casper strain embryos at the one cell stage. An approximate volume of 1–2 nl and 60 ng/ml concentration for both plasmid and RNA was used for injections. The fish with the most labeled neurons were selected to be outcrossed so their offspring could be screened for transgenic founders. A transgenic founder with mostly uniform labeling of the sensory neurons with EB3-GFP at an expression level that enabled imaging of EB comets was selected, and its progeny were used for imaging experiments.

Zebrafish mounting and live imaging
For zebrafish live imaging, larval fish (48 to 96 hpf) were anesthetized in 0.4% tricaine and embedded in 1.5% low melt agarose containing 0.4% tricaine and positioned on a glass coverslip. EB3-GFP comet videos were collected with a 63×/1.4 NA Plan Apochromat oil immersion objective on a Zeiss Imager M2 with a Zeiss AxioCam 506 camera using Zeiss Zen Blue software version 2.3. Overview images were collected with 10×/0.3 NA EC Plan-Neofluar objective or 63×/1.4 NA Plan Apochromat oil immersion objective on an inverted Zeiss LSM800 confocal microscope. To provide a cell shape marker for cell morphology, the P2X3.E1B:LexA-VP16.Sv40.4XLexAop.E1B:EB3-GFP.Sv40 fish described above were crossed to P2X3.E1B:LexA-VP16.Sv40.4xLexAop.E1B:mCherry.Sv40, ISL1.E1B:LexA-VP16.Sv40.4xLexAop.E1B:tdTomato.SV40 fish.

Drosophila larval live imaging
For Drosophila live imaging, 3-d-old larvae were mounted between a dried-agarose–coated microscope slide and a coverslip for immobilization. The larva was immobilized by gentle pressure from the coverslip, which was held down with sticky tape. All imaging was performed at room temperature. To study dendrite microtubule polarity, EB1-GFP videos were recorded using a widefield Zeiss Imager M2 microscope with AxioCam M2 or AxioCam 506 camera under 63× 1.4 NA Plan Apochromat oil immersion objective. A Colibri2 LED illumination system and Zeiss Zen Blue software were used to perform one frame per second, 300-frame recordings (Fig. 1, Fig. 4, and Fig. 5). Videos were exported, inverted, aligned, and analyzed with ImageJ software (https://imagej.nih.gov/ij/). Kymographs were generated with the MultipleKymograph ImageJ plugin. At least two kymographs, one with line width one and another with line width three, were generated from each video. EB1 comet numbers were counted manually from videos and confirmed with analysis of kymographs. As each cell contains limited numbers of growing microtubules, data from all cells were pooled to generate the fraction of comets moving toward or away from the cell body in all neurons. For dendrite branch analysis of ddaC

neurons, only thick dendritic branches close to cell body were included for quantification. Dendrite branches were classified as plus-end-out if >90% of EB1-GFP comets move away from the cell body, minus-end-out if >90% of EB1-GFP comets moved toward the cell body, and mixed for intermediate values.

For analysis of dendrite tips, secondary dendrites of ddaE neuron without branches were sampled. A 221-Gal4, UAS-EB1-TagRFP-T tester line was crossed to YFP-Patronin, Patronin-Venus (Nashchekin et al., 2016), or EGFP-Patronin (Takeda et al., 2018), and videos were obtained on a Zeiss LSM800 microscope.

All other imaging experiments were performed with confocal microscopes, including an inverted Zeiss LSM700, an inverted Zeiss LSM800 (both of these were equipped with manual MicroPoint laser systems [Andor Technology] to perform injury), or an upright Zeiss LSM800. Time-lapse recording of EB1-GFP or EB1-TagRFP-T was performed with a 63× 1.4 NA oil objective using at 0.5 frames per second for 5 min, or 20 min for minus end polymerization studies shown in Fig. 3 and Fig. 5. Quantification of minus end growth length, duration, and speed was done based on kymograph measurements. To quantify the density of plus ends, the number of microtubule plus ends in a 200-s video was divided by the length of in-focus dendrite. The values were multiplied by 10 to give the minus end number per 10 µm. Similar measurements were done for minus end density (Fig. 6 E), except the number of minus ends was quantified from 5-min videos. Overview images were generated using the tiling function of Zeiss Zen Blue software.

The kymograph in Fig. S1 A was generated from data acquired using the AiryScan detector and processing on a Zeiss LSM800 upright microscope acquired with a Plan Apochromat 63× 1.4 NA oil objective.

Drosophila larval immunostaining
Third-instar larva were dissected and stained as previously described (Nguyen et al., 2011; Tao et al., 2016). Briefly, larvae were dissected in Schneider's medium followed by fixation in 4% PFA for 30 min. Then larval fillets were washed/permeabilized three times for a total of 20 min in permeabilizing buffer (PBS and 0.2% Triton). Next, larval fillets were incubated in blocking buffer (PBS, 0.2% Triton, 10% normal goat serum, and 2% BSA) at room temperature for 1 h. Larvae were then incubated with primary antibody overnight at 4°C. Five washes with blocking buffer were applied the next day, followed by incubation with secondary antibody for 2 h at room temperature. Final washes with blocking buffer were performed before imaging. For EB1 staining, third instar larvae were collected from crossing tester line UAS-YFP-Patronin; 221-Gal4, UAS-dicer2 to control or EB1 RNAi flies. EB1 antibody (a gift from S. Rogers, University of North Carolina, Chapel Hill, NC) was diluted 1:100 in blocking buffer. Cy5 goat anti-rabbit (Life Technologies) secondary antibody was diluted 1:100 in blocking buffer. For MAP1B/futsch staining, third instar larvae were collected from crossing tester line UAS-mCD8-RFP; 221-Gal4 to control or Patronin RNAi BL36659 flies. 22C10 (Developmental Studies Hybridoma Bank) antibody was diluted 1:10 in blocking buffer. Rhodamine-Red-X-coupled secondary antibody (Jackson ImmunoResearch) was diluted 1:100 in blocking buffer.

To quantify 22C10 (futsch) FI, z-stack images of control or Patronin RNAi neurons were acquired with the same settings. After maximum projection of each imaged neuron, raw FI was measured along dendrites (50 µm from the base of a dendrite) and axons (15 µm from the base of axon) of ddaE neurons. FI of a neighboring ciliated dendrite was used for normalization to account for regional differences in staining efficiency.

Drosophila embryo imaging

To study microtubule polarity in developing neurons, the 1407-Gal4, UAS-EB1-GFP; UAS-dicer2 tester line was crossed to control or Patronin RNAi lines. Embryos were collected from apple juice agar caps supplied with yeast paste for a 24-h window at 25°C. Embryos were carefully transferred to a mesh-bottom chamber using a fine paintbrush and then dechorionated with 50% bleach for 2 min, fully rinsed, and transferred to a 1.5-ml centrifuge tube containing 0.5 ml of heptane. Next, embryos were placed on a coverslip to make a single layer. Immediately after heptane evaporated, embryos were covered with a thin layer of halocarbon oil 27 (Sigma-Aldrich). The coverslip with embryos was then taped to a metal microscope slide with an open window in the middle. Images and videos were recorded as described above with Zeiss LSM800 upright microscope.

Dendrite injury and regeneration

To study microtubule polarity in regenerating ddaC dendrites, the 477-Gal4, UAS-EB1-GFP/CyO; UAS-dicer2 tester line was crossed with control or Patronin RNAi fly lines. 3-d-old larvae were collected from cornmeal food caps to perform a dendrite severing assay. A mounted larva was visualized under 63× 1.4 NA oil objective with a LSM700 microscope, and a MicroPoint pulsed UV laser was used to sever all the dendrites at their base. Larvae were then allowed to recover on food caps at 25°C for the times indicated before being assayed for dendrite regeneration and microtubule polarity.

To assess dendrite regeneration flies from the UAS-dicer2; ppk-Gal4, UAS-mCD8-GFP tester line were crossed with control or Patronin RNAi flies. Dendrite removal was performed as above. Injured neurons were reimaged with an LSM800 upright microscope 24 h after injury, and the longest diameter across the regenerating dendrite arbor was measured for each neuron.

To visualize minus end growth in regenerating dendrites, UAS-YFP-Patronin/CyO-pAct-GFP; UAS-EB1-TagRFP-T/TM6 flies were crossed with 477-Gal4 flies. Dendrite removal was performed as above, and EB1-TagRFP-T and YFP-Patronin were recorded at 0.5 frames per second for 5 min.

To probe stable microtubules, images were acquired immediately after severing. UAS-mCD8-RFP; 221-Gal4 flies were crossed with UAS-YFP-Patronin flies, and the comb dendrite of ddaE was cut. To study microtubule polarity adjacent to the severing site, UAS-YFP-Patronin/Cyo-pAct-GFP; 221-Gal4, UAS-EB1-TagRFP-T, UAS-dicer2 flies were crossed to control RNAi flies, and the dendrite was severed.

RNAi knockdown efficiency tests

UAS-YFP-Patronin/CyO-pAct-GFP; 221-Gal4, UAS-dicer2, UAS-EB1-TagRFP-T flies were crossed with control, Patronin RNAi VDRC27654, Patronin RNAi BL36659, or EB1 RNAi VDRC24451 flies. Images of all genotypes were acquired with the same settings. FIs of YFP-Patronin and EB1-TagRFP-T were measured in the cell body after maximum projection of each imaged neuron. Then the experimental FI values were divided by the mean FI of control neurons. Mean and SD were calculated from normalized values.

To test the efficiency of Patronin RNAi against endogenous Patronin protein, we took advantage of the endogenously tagged Patronin-Venus fly line generated by the CRISPR-Cas9 system (Nashchekin et al., 2016). Either ppk-Gal4, UAS-TagRFP-T or ppk-Gal4, UAS-TagRFP-T, UAS-Patronin RNAi 2 flies were crossed to Patronin-Venus flies. Z-stacks of ddaC neurons were obtained on LSM 800 upright microscope with 63×/1.4 NA Plan Apochromat oil immersion objective. FI of ddaC cell body and adjacent nonneuron area were measured on maximum projection of z-stacks. Normalized FIs of ddaC cell body were calculated by subtracting FIs of adjacent nonneuron areas. Each normalized ddaC cell body FI was divided by the mean FI of the control group. Mean and SD of control and Patronin RNAi groups were then plotted.

Class IV ddaC dendrite morphology analysis

The tester fly line UAS-dicer2; ppk-Gal4, UAS-mCD8-GFP was crossed with control or Patronin RNAi line VDRC27654. Tiled images were generated with a 63×/1.4 NA Plan Apochromat oil immersion objective on an upright LSM800 microscope using Zeiss Zen Blue software. We used the Simple Neuron Tracer plugin in Fiji to trace and label every dendrite of each ddaC neuron, exported traces data to Excel, and calculated the total dendrite length. The Sholl analysis plugin in Fiji was used to generate dendrite complexity data.

To study ddaE neuron morphology, we used a Patronin transheterozygous mutant as described above with EB1-GFP as the cell shape marker. A binary classification of normal or abnormal morphology was applied to a total of 72 neurons imaged from 12 larvae. One exception that was classified as abnormal morphology had no ddaE neuron in the hemisegment.

Estimating relative protein expression levels from different tagged Patronin lines

We used Patronin tagged with Venus, 3xYFP, and EGFP. Images of larvae containing each transgene were acquired with the same settings. To compare intensity across fluorophores, we generated a conversion factor based on percent absorbance at the excitation wavelength, the extinction coefficient, the quantum yield of each florescent protein, and the proportion of their emission within the collection window of 495 to 529 nm. The photophysical properties were acquired from the website http://FPbase.org. Additionally, given that fluorescent protein multimers result in an increase in brightness that is not quite linear with copy number (Shearin et al., 2014; Dunsing et al., 2018), we used a multiplier of 2.25× rather than 3× when estimating the expected brightness of the 3xYFP fusion. The normalization equation and results are shown below. Relative signal per molecule represents the efficiency of emission compared with a perfect fluorophore. (*Extinction Coefficient*) × (*Percent Absorbance*

at 488 nm) × (Quantum Yield) × (Proportion of Emission between 495 and 529 nm) = Relative Signal per Molecule.

$$\frac{Signal\ Collected}{Relative\ Signal\ Per\ molecule} = Relative\ Expression\ Level.$$

Values calculated for each fluorophore and tagged protein are shown in Table S2. The Patronin-Venus was present at the endogenous locus on one chromosome, and so the baseline Patronin expression level would be equivalent to 2× the brightness of this signal. When converted to relative fluorescent level, the baseline amount of Patronin would be 2 × (0.476), which is then set to 1. The other two tagged Patronin transgenes are at different loci, and so would be added on top of the baseline expression level. These total expression levels (untagged + tagged Patronin) are shown in Fig. 6 G.

Small molecule inhibitors of JNK signaling pathway

We used SP600125 at 1 mM in cornmeal fly food based on other reports (Hong et al., 2012), as well as in a laboratory dosage test. 0.5% DMSO was included for better solubility. 50 mM GNE-3511 was used in cornmeal fly food with 0.5% DMSO. Fly food containing 0.5% DMSO was used as vehicle control. The tester line 221-Gal4, UAS-dicer2, UAS-EB1-TagRFP-T, puc-GFP/TM6 was crossed to control or Patronin RNAi fly lines. After aging larvae for 2 d on standard food caps, animals were transferred to drug or vehicle control food and allowed to grow for another day. 3-d-old larvae were imaged for puc-GFP FI readings, microtubule polarity, and microtubule dynamics.

Statistical methods

Statistics were performed with GraphPad Prism 7 software. Statistical methods were chosen based on the data type, and the analysis used in each case is detailed in each figure legend. In all figures where error bars are present, these represent the SD.

Online supplemental material

Fig. S1 includes a kymograph of Patronin-Venus as well as images showing knockdown of Patronin and EB1. Fig. S2 shows quantitation of minus end behavior using tagged Patronin. Fig. S3 includes images of stable microtubules in control and Patronin knockdown neurons as well as quantitation of plus end behavior in control and Patronin knockdown cells. Fig. S4 shows additional assays to probe behavior of stable microtubules in control and Patronin knockdown neurons. Fig. S5 includes analysis of microtubule behavior in Patronin mutant neurons as well as cell shape in Patronin RNAi and mutant neurons. Video 1 is of a ddaE neuron expressing EB1-GFP to monitor growing microtubule ends. Video 2 shows part of a ddaE dendrite expressing EB1-GFP. Video 3 is of microtubule dynamics in the sensory endings of a zebrafish RB neuron. Video 4 shows EB1-TagRFP-T and YFP-Patronin dynamics side by side in a region of a ddaE dendrite. Video 5 has EB1-GFP dynamics in control and Patronin RNAi ddaE neurons. Video 6 compares EB1-GFP dynamics in control and Patronin RNAi ddaC neurons. Video 7 includes EB1-GFP dynamics in ddaE neurons at different stages of development. Video 8 is of microtubule dynamics in a Patronin RNAi ddaE neuron late in dendrite development. Video 9 shows EB1-TagRFP-T and

YFP-Patronin behavior in regenerating dendrites. Video 10 is of microtubule dynamics in control and Patronin RNAi ddaC neurons during dendrite regeneration. Table S1 is a list of reagents used in this study. Table S2 shows calculations of relative expression level for each Patronin transgene used.

References

Akhmanova, A., and C.C. Hoogenraad. 2015. Microtubule minus-end-targeting proteins. *Curr. Biol.* 25:R162–R171. https://doi.org/10.1016/j.cub.2014.12.027

Akhmanova, A., and M.O. Steinmetz. 2015. Control of microtubule organization and dynamics: two ends in the limelight. *Nat. Rev. Mol. Cell Biol.* 16:711–726. https://doi.org/10.1038/nrm4084

Baas, P.W., and S. Lin. 2011. Hooks and comets: The story of microtubule polarity orientation in the neuron. *Dev. Neurobiol.* 71:403–418. https://doi.org/10.1002/dneu.20818

Baas, P.W., A. Karabay, and L. Qiang. 2005. Microtubules cut and run. *Trends Cell Biol.* 15:518–524. https://doi.org/10.1016/j.tcb.2005.08.004

Bellen, H.J., R.W. Levis, G. Liao, Y. He, J.W. Carlson, G. Tsang, M. Evans-Holm, P.R. Hiesinger, K.L. Schulze, G.M. Rubin, et al. 2004. The BDGP gene disruption project: single transposon insertions associated with 40% of Drosophila genes. *Genetics.* 167:761–781. https://doi.org/10.1534/genetics.104.026427

Bennett, B.L., D.T. Sasaki, B.W. Murray, E.C. O'Leary, S.T. Sakata, W. Xu, J.C. Leisten, A. Motiwala, S. Pierce, Y. Satoh, et al. 2001. SP600125, an anthrapyrazolone inhibitor of Jun N-terminal kinase. *Proc. Natl. Acad. Sci. USA.* 98:13681–13686. https://doi.org/10.1073/pnas.251194298

Bieling, P., L. Laan, H. Schek, E.L. Munteanu, L. Sandblad, M. Dogterom, D. Brunner, and T. Surrey. 2007. Reconstitution of a microtubule plus-end tracking system in vitro. *Nature.* 450:1100–1105. https://doi.org/10.1038/nature06386

Brouhard, G.J. 2015. Dynamic instability 30 years later: complexities in microtubule growth and catastrophe. *Mol. Biol. Cell.* 26:1207–1210. https://doi.org/10.1091/mbc.E13-10-0594

Chen, J., C. Xie, L. Tian, L. Hong, X. Wu, and J. Han. 2010. Participation of the p38 pathway in Drosophila host defense against pathogenic bacteria and fungi. *Proc. Natl. Acad. Sci. USA.* 107:20774–20779. https://doi.org/10.1073/pnas.1009223107

Chen, L., M.C. Stone, J. Tao, and M.M. Rolls. 2012. Axon injury and stress trigger a microtubule-based neuroprotective pathway. *Proc. Natl. Acad. Sci. USA.* 109:11842–11847. https://doi.org/10.1073/pnas.1121180109

Chintapalli, V.R., J. Wang, and J.A. Dow. 2007. Using FlyAtlas to identify better Drosophila melanogaster models of human disease. *Nat. Genet.* 39:715–720. https://doi.org/10.1038/ng2049

Chuang, M., A. Goncharov, S. Wang, K. Oegema, Y. Jin, and A.D. Chisholm. 2014. The microtubule minus-end-binding protein patronin/PTRN-1 is required for axon regeneration in C. elegans. *Cell Reports.* 9:874–883. https://doi.org/10.1016/j.celrep.2014.09.054

Dammermann, A., A. Desai, and K. Oegema. 2003. The minus end in sight. *Curr. Biol.* 13:R614–R624. https://doi.org/10.1016/S0960-9822(03)00530-X

Del Castillo, U., W. Lu, M. Winding, M. Lakonishok, and V.I. Gelfand. 2015. Pavarotti/MKLP1 regulates microtubule sliding and neurite outgrowth in Drosophila neurons. *Curr. Biol.* 25:200–205. https://doi.org/10.1016/j.cub.2014.11.008

Dietzl, G., D. Chen, F. Schnorrer, K.C. Su, Y. Barinova, M. Fellner, B. Gasser, K. Kinsey, S. Oppel, S. Scheiblauer, et al. 2007. A genome-wide transgenic RNAi library for conditional gene inactivation in Drosophila. *Nature.* 448:151–156. https://doi.org/10.1038/nature05954

Distel, M., J.C. Hocking, K. Volkmann, and R.W. Köster. 2010. The centrosome neither persistently leads migration nor determines the site of axonogenesis in migrating neurons in vivo. *J. Cell Biol.* 191:875–890. https://doi.org/10.1083/jcb.201004154

Dunsing, V., M. Luckner, B. Zühlke, R.A. Petazzi, A. Herrmann, and S. Chiantia. 2018. Optimal fluorescent protein tags for quantifying protein oligomerization in living cells. *Sci. Rep.* 8:10634. https://doi.org/10.1038/s41598-018-28858-0

Gardner, M.K., M. Zanic, and J. Howard. 2013. Microtubule catastrophe and rescue. *Curr. Opin. Cell Biol.* 25:14–22. https://doi.org/10.1016/j.ceb.2012.09.006

Goodwin, S.S., and R.D. Vale. 2010. Patronin regulates the microtubule network by protecting microtubule minus ends. *Cell.* 143:263–274. https://doi.org/10.1016/j.cell.2010.09.022

Goodwin, P.R., J.M. Sasaki, and P. Juo. 2012. Cyclin-dependent kinase 5 regulates the polarized trafficking of neuropeptide-containing dense-core vesicles in Caenorhabditis elegans motor neurons. *J. Neurosci.* 32:8158–8172. https://doi.org/10.1523/JNEUROSCI.0251-12.2012

Grueber, W.B., L.Y. Jan, and Y.N. Jan. 2003a. Different levels of the homeodomain protein cut regulate distinct dendrite branching patterns of Drosophila multidendritic neurons. *Cell.* 112:805–818. https://doi.org/10.1016/S0092-8674(03)00160-0

Grueber, W.B., B. Ye, A.W. Moore, L.Y. Jan, and Y.N. Jan. 2003b. Dendrites of distinct classes of Drosophila sensory neurons show different capacities for homotypic repulsion. *Curr. Biol.* 13:618–626. https://doi.org/10.1016/S0960-9822(03)00207-0

Harterink, M., S.L. Edwards, B. de Haan, K.W. Yau, S. van den Heuvel, L.C. Kapitein, K.G. Miller, and C.C. Hoogenraad. 2018. Local microtubule organization promotes cargo transport in C. elegans dendrites. *J. Cell Sci.* 131:jcs223107. https://doi.org/10.1242/jcs.223107

Hendershott, M.C., and R.D. Vale. 2014. Regulation of microtubule minus-end dynamics by CAMSAPs and Patronin. *Proc. Natl. Acad. Sci. USA.* 111:5860–5865. https://doi.org/10.1073/pnas.1404133111

Hill, S.E., M. Parmar, K.W. Gheres, M.A. Guignet, Y. Huang, F.R. Jackson, and M.M. Rolls. 2012. Development of dendrite polarity in Drosophila neurons. *Neural Dev.* 7:34. https://doi.org/10.1186/1749-8104-7-34

Hong, Y.K., S. Lee, S.H. Park, J.H. Lee, S.Y. Han, S.T. Kim, Y.K. Kim, S. Jeon, B.S. Koo, and K.S. Cho. 2012. Inhibition of JNK/dFOXO pathway and caspases rescues neurological impairments in Drosophila Alzheimer's disease model. *Biochem. Biophys. Res. Commun.* 419:49–53. https://doi.org/10.1016/j.bbrc.2012.01.122

Hughes, C.L., and J.B. Thomas. 2007. A sensory feedback circuit coordinates muscle activity in Drosophila. *Mol. Cell. Neurosci.* 35:383–396. https://doi.org/10.1016/j.mcn.2007.04.001

Hummel, T., K. Krukkert, J. Roos, G. Davis, and C. Klämbt. 2000. Drosophila Futsch/22C10 is a MAP1B-like protein required for dendritic and axonal development. *Neuron.* 26:357–370. https://doi.org/10.1016/S0896-6273(00)81169-1

Jiang, K., S. Hua, R. Mohan, I. Grigoriev, K.W. Yau, Q. Liu, E.A. Katrukha, A.F. Altelaar, A.J. Heck, C.C. Hoogenraad, and A. Akhmanova. 2014. Microtubule minus-end stabilization by polymerization-driven CAMSAP deposition. *Dev. Cell.* 28:295–309. https://doi.org/10.1016/j.devcel.2014.01.001

Jiang, K., L. Rezabkova, S. Hua, Q. Liu, G. Capitani, A.F.M. Altelaar, A.J.R. Heck, R.A. Kammerer, M.O. Steinmetz, and A. Akhmanova. 2017. Microtubule minus-end regulation at spindle poles by an ASPM-katanin complex. *Nat. Cell Biol.* 19:480–492. https://doi.org/10.1038/ncb3511

King, M.D., G.W. Phillips, P.A. Bignone, N.V. Hayes, J.C. Pinder, and A.J. Baines. 2014. A conserved sequence in calmodulin regulated spectrin-associated protein 1 links its interaction with spectrin and calmodulin to neurite outgrowth. *J. Neurochem.* 128:391–402. https://doi.org/10.1111/jnc.12462

Kleele, T., P. Marinković, P.R. Williams, S. Stern, E.E. Weigand, P. Engerer, R. Naumann, J. Hartmann, R.M. Karl, F. Bradke, et al. 2014. An assay to image neuronal microtubule dynamics in mice. *Nat. Commun.* 5:4827. https://doi.org/10.1038/ncomms5827

Lee, T.J., J.W. Lee, E.M. Haynes, K.W. Eliceiri, and M.C. Halloran. 2017. The Kinesin Adaptor Calsyntenin-1 Organizes Microtubule Polarity and Regulates Dynamics during Sensory Axon Arbor Development. *Front. Cell. Neurosci.* 11:107. https://doi.org/10.3389/fncel.2017.00107

Lin, S., M. Liu, O.I. Mozgova, W. Yu, and P.W. Baas. 2012. Mitotic motors coregulate microtubule patterns in axons and dendrites. *J. Neurosci.* 32:14033–14049. https://doi.org/10.1523/JNEUROSCI.3070-12.2012

Luo, L., Y.J. Liao, L.Y. Jan, and Y.N. Jan. 1994. Distinct morphogenetic functions of similar small GTPases: Drosophila Drac1 is involved in axonal outgrowth and myoblast fusion. *Genes Dev.* 8:1787–1802. https://doi.org/10.1101/gad.8.15.1787

Marcette, J.D., J.J. Chen, and M.L. Nonet. 2014. The Caenorhabditis elegans microtubule minus-end binding homolog PTRN-1 stabilizes synapses and neurites. *eLife.* 3:e01637. https://doi.org/10.7554/eLife.01637

Massaro, C.M., J. Pielage, and G.W. Davis. 2009. Molecular mechanisms that enhance synapse stability despite persistent disruption of the spectrin/ankyrin/microtubule cytoskeleton. *J. Cell Biol.* 187:101–117. https://doi.org/10.1083/jcb.200903166

Mattie, F.J., M.M. Stackpole, M.C. Stone, J.R. Clippard, D.A. Rudnick, Y. Qiu, J. Tao, D.L. Allender, M. Parmar, and M.M. Rolls. 2010. Directed microtubule growth, +TIPs, and kinesin-2 are required for uniform microtubule polarity in dendrites. *Curr. Biol.* 20:2169–2177. https://doi.org/10.1016/j.cub.2010.11.050

Meng, W., Y. Mushika, T. Ichii, and M. Takeichi. 2008. Anchorage of microtubule minus ends to adherens junctions regulates epithelial cell-cell contacts. *Cell.* 135:948–959. https://doi.org/10.1016/j.cell.2008.09.040

Mimori-Kiyosue, Y., I. Grigoriev, G. Lansbergen, H. Sasaki, C. Matsui, F. Severin, N. Galjart, F. Grosveld, I. Vorobjev, S. Tsukita, and A. Akhmanova. 2005. CLASP1 and CLASP2 bind to EB1 and regulate microtubule plus-end dynamics at the cell cortex. *J. Cell Biol.* 168:141–153. https://doi.org/10.1083/jcb.200405094

Mitchison, T., and M. Kirschner. 1984. Dynamic instability of microtubule growth. *Nature.* 312:237–242. https://doi.org/10.1038/312237a0

Muhia, M., E. Thies, D. Labonté, A.E. Ghiretti, K.V. Gromova, F. Xompero, C. Lappe-Siefke, I. Hermans-Borgmeyer, D. Kuhl, M. Schweizer, et al. 2016. The Kinesin KIF21B Regulates Microtubule Dynamics and Is Essential for Neuronal Morphology, Synapse Function, and Learning and Memory. *Cell Reports.* 15:968–977. https://doi.org/10.1016/j.celrep.2016.03.086

Nakamura, M., J.J. Lindeboom, M. Saltini, B.M. Mulder, and D.W. Ehrhardt. 2018. SPR2 protects minus ends to promote severing and reorientation of plant cortical microtubule arrays. *J. Cell Biol.* 217:915–927. https://doi.org/10.1083/jcb.201708130

Nashchekin, D., A.R. Fernandes, and D. St Johnston. 2016. Patronin/Shot Cortical Foci Assemble the Noncentrosomal Microtubule Array that Specifies the Drosophila Anterior-Posterior Axis. *Dev. Cell.* 38:61–72. https://doi.org/10.1016/j.devcel.2016.06.010

Nechipurenko, I.V., and H.T. Broihier. 2012. FoxO limits microtubule stability and is itself negatively regulated by microtubule disruption. *J. Cell Biol.* 196:345–362. https://doi.org/10.1083/jcb.201105154

Nguyen, M.M., M.C. Stone, and M.M. Rolls. 2011. Microtubules are organized independently of the centrosome in Drosophila neurons. *Neural Dev.* 6:38. https://doi.org/10.1186/1749-8104-6-38

Nguyen, M.M., C.J. McCracken, E.S. Milner, D.J. Goetschius, A.T. Weiner, M.K. Long, N.L. Michael, S. Munro, and M.M. Rolls. 2014. Γ-tubulin controls neuronal microtubule polarity independently of Golgi outposts. *Mol. Biol. Cell.* 25:2039–2050. https://doi.org/10.1091/mbc.e13-09-0515

Noordstra, I., Q. Liu, W. Nijenhuis, S. Hua, K. Jiang, M. Baars, S. Remmelzwaal, M. Martin, L.C. Kapitein, and A. Akhmanova. 2016. Control of apico-basal epithelial polarity by the microtubule minus-end-binding protein CAMSAP3 and spectraplakin ACF7. *J. Cell Sci.* 129:4278–4288. https://doi.org/10.1242/jcs.194878

Ori-McKenney, K.M., L.Y. Jan, and Y.N. Jan. 2012. Golgi outposts shape dendrite morphology by functioning as sites of acentrosomal microtubule nucleation in neurons. *Neuron.* 76:921–930. https://doi.org/10.1016/j.neuron.2012.10.008

Palanca, A.M., S.L. Lee, L.E. Yee, C. Joe-Wong, A. Trinh, E. Hiroyasu, M. Husain, S.E. Fraser, M. Pellegrini, and A. Sagasti. 2013. New transgenic reporters identify somatosensory neuron subtypes in larval zebrafish. *Dev. Neurobiol.* 73:152–167. https://doi.org/10.1002/dneu.22049

Patel, S., F. Cohen, B.J. Dean, K. De La Torre, G. Deshmukh, A.A. Estrada, A.S. Ghosh, P. Gibbons, A. Gustafson, M.P. Huestis, et al. 2015. Discovery of dual leucine zipper kinase (DLK, MAP3K12) inhibitors with activity in neurodegeneration models. *J. Med. Chem.* 58:401–418. https://doi.org/10.1021/jm5013984

Richardson, C.E., K.A. Spilker, J.G. Cueva, J. Perrino, M.B. Goodman, and K. Shen. 2014. PTRN-1, a microtubule minus end-binding CAMSAP homolog, promotes microtubule function in Caenorhabditis elegans neurons. *eLife.* 3:e01498. https://doi.org/10.7554/eLife.01498

Rogers, S.L., G.C. Rogers, D.J. Sharp, and R.D. Vale. 2002. Drosophila EB1 is important for proper assembly, dynamics, and positioning of the mitotic spindle. *J. Cell Biol.* 158:873–884. https://doi.org/10.1083/jcb.200202032

Rolls, M.M., D. Satoh, P.J. Clyne, A.L. Henner, T. Uemura, and C.Q. Doe. 2007. Polarity and intracellular compartmentalization of Drosophila neurons. *Neural Dev.* 2:7. https://doi.org/10.1186/1749-8104-2-7

Sánchez-Huertas, C., F. Freixo, R. Viais, C. Lacasa, E. Soriano, and J. Lüders. 2016. Non-centrosomal nucleation mediated by augmin organizes microtubules in post-mitotic neurons and controls axonal microtubule polarity. *Nat. Commun.* 7:12187. https://doi.org/10.1038/ncomms12187

Shaner, N.C., M.Z. Lin, M.R. McKeown, P.A. Steinbach, K.L. Hazelwood, M.W. Davidson, and R.Y. Tsien. 2008. Improving the photostability of bright monomeric orange and red fluorescent proteins. *Nat. Methods.* 5:545–551. https://doi.org/10.1038/nmeth.1209

Sharp, D.J., and J.L. Ross. 2012. Microtubule-severing enzymes at the cutting edge. *J. Cell Sci.* 125:2561–2569. https://doi.org/10.1242/jcs.101139

Sharp, D.J., W. Yu, L. Ferhat, R. Kuriyama, D.C. Rueger, and P.W. Baas. 1997. Identification of a microtubule-associated motor protein essential for dendritic differentiation. *J. Cell Biol.* 138:833–843. https://doi.org/10.1083/jcb.138.4.833

Shaw, S.L., R. Kamyar, and D.W. Ehrhardt. 2003. Sustained microtubule treadmilling in Arabidopsis cortical arrays. *Science.* 300:1715–1718. https://doi.org/10.1126/science.1083529

Shearin, H.K., I.S. Macdonald, L.P. Spector, and R.S. Stowers. 2014. Hexameric GFP and mCherry reporters for the Drosophila GAL4, Q, and LexA transcription systems. *Genetics.* 196:951–960. https://doi.org/10.1534/genetics.113.161141

Stepanova, T., J. Slemmer, C.C. Hoogenraad, G. Lansbergen, B. Dortland, C.I. De Zeeuw, F. Grosveld, G. van Cappellen, A. Akhmanova, and N. Galjart. 2003. Visualization of microtubule growth in cultured neurons via the use of EB3-GFP (end-binding protein 3-green fluorescent protein). *J. Neurosci.* 23:2655–2664. https://doi.org/10.1523/JNEUROSCI.23-07-02655.2003

Stepanova, T., I. Smal, J. van Haren, U. Akinci, Z. Liu, M. Miedema, R. Limpens, M. van Ham, M. van der Reijden, R. Poot, et al. 2010. History-dependent catastrophes regulate axonal microtubule behavior. *Curr. Biol.* 20:1023–1028. https://doi.org/10.1016/j.cub.2010.04.024

Stiess, M., N. Maghelli, L.C. Kapitein, S. Gomis-Rüth, M. Wilsch-Bräuninger, C.C. Hoogenraad, I.M. Tolić-Nørrelykke, and F. Bradke. 2010. Axon extension occurs independently of centrosomal microtubule nucleation. *Science.* 327:704–707. https://doi.org/10.1126/science.1182179

Stone, M.C., F. Roegiers, and M.M. Rolls. 2008. Microtubules have opposite orientation in axons and dendrites of Drosophila neurons. *Mol. Biol. Cell.* 19:4122–4129. https://doi.org/10.1091/mbc.e07-10-1079

Stone, M.C., R.M. Albertson, L. Chen, and M.M. Rolls. 2014. Dendrite injury triggers DLK-independent regeneration. *Cell Reports.* 6:247–253. https://doi.org/10.1016/j.celrep.2013.12.022

Takeda, M., M.M. Sami, and Y.C. Wang. 2018. A homeostatic apical microtubule network shortens cells for epithelial folding via a basal polarity shift. *Nat. Cell Biol.* 20:36–45. https://doi.org/10.1038/s41556-017-0001-3

Tao, J., C. Feng, and M.M. Rolls. 2016. The microtubule-severing protein fidgetin acts after dendrite injury to promote their degeneration. *J. Cell Sci.* 129:3274–3281. https://doi.org/10.1242/jcs.188540

Tas, R.P., A. Chazeau, B.M.C. Cloin, M.L.A. Lambers, C.C. Hoogenraad, and L.C. Kapitein. 2017. Differentiation between Oppositely Oriented Microtubules Controls Polarized Neuronal Transport. *Neuron.* 96:1264–1271. https://doi.org/10.1016/j.neuron.2017.11.018

Toya, M., S. Kobayashi, M. Kawasaki, G. Shioi, M. Kaneko, T. Ishiuchi, K. Misaki, W. Meng, and M. Takeichi. 2016. CAMSAP3 orients the apical-to-basal polarity of microtubule arrays in epithelial cells. *Proc. Natl. Acad. Sci. USA.* 113:332–337. https://doi.org/10.1073/pnas.1520638113

Valakh, V., L.J. Walker, J.B. Skeath, and A. DiAntonio. 2013. Loss of the spectraplakin short stop activates the DLK injury response pathway in Drosophila. *J. Neurosci.* 33:17863–17873. https://doi.org/10.1523/JNEUROSCI.2196-13.2013

Wang, S., D. Wu, S. Quintin, R.A. Green, D.K. Cheerambathur, S.D. Ochoa, A. Desai, and K. Oegema. 2015. NOCA-1 functions with γ-tubulin and in parallel to Patronin to assemble non-centrosomal microtubule arrays in C. elegans. *eLife.* 4:e08649. https://doi.org/10.7554/eLife.08649

Wiese, C. 2008. Distinct Dgrip84 isoforms correlate with distinct gamma-tubulins in Drosophila. *Mol. Biol. Cell.* 19:368–377. https://doi.org/10.1091/mbc.e07-08-0801

Wittmann, T., A. Hyman, and A. Desai. 2001. The spindle: a dynamic assembly of microtubules and motors. *Nat. Cell Biol.* 3:E28–E34. https://doi.org/10.1038/35050669

Xiong, X., X. Wang, R. Ewanek, P. Bhat, A. Diantonio, and C.A. Collins. 2010. Protein turnover of the Wallenda/DLK kinase regulates a retrograde response to axonal injury. *J. Cell Biol.* 191:211–223. https://doi.org/10.1083/jcb.201006039

Yau, K.W., S.F. van Beuningen, I. Cunha-Ferreira, B.M. Cloin, E.Y. van Battum, L. Will, P. Schätzle, R.P. Tas, J. van Krugten, E.A. Katrukha, et al. 2014. Microtubule minus-end binding protein CAMSAP2 controls axon specification and dendrite development. *Neuron.* 82:1058–1073. https://doi.org/10.1016/j.neuron.2014.04.019

Yau, K.W., P. Schätzle, E. Tortosa, S. Pagès, A. Holtmaat, L.C. Kapitein, and C.C. Hoogenraad. 2016. Dendrites In Vitro and In Vivo Contain Microtubules of Opposite Polarity and Axon Formation Correlates with Uniform Plus-End-Out Microtubule Orientation. *J. Neurosci.* 36:1071–1085. https://doi.org/10.1523/JNEUROSCI.2430-15.2016

Yu, W., D.J. Sharp, R. Kuriyama, P. Mallik, and P.W. Baas. 1997. Inhibition of a mitotic motor compromises the formation of dendrite-like processes from neuroblastoma cells. *J. Cell Biol.* 136:659–668. https://doi.org/10.1083/jcb.136.3.659

Yu, W., C. Cook, C. Sauter, R. Kuriyama, P.L. Kaplan, and P.W. Baas. 2000. Depletion of a microtubule-associated motor protein induces the loss of dendritic identity. *J. Neurosci.* 20:5782–5791. https://doi.org/10.1523/JNEUROSCI.20-15-05782.2000